*mathematics*

MDPI

*Article*

# Modeling a Multi-Lane Highway System Considering the Combined Impacts of Overtaking Mechanisms and Aggressive Lane-Changing Behaviors

**Shuhong Yang [1,2], Bin Huang [2,*], Chuan Tian [1] and Yirong Kang [3]**

[1] Guizhou Provincial Research Center for Collaborative Intelligent Perception of Mountain Spatial Information, Guizhou University of Commerce, Guiyang 550014, China; ysh@gzcc.edu.cn (S.Y.); tcgzuc2024@gzcc.edu.cn (C.T.)
[2] School of Computer and Information Engineering, Guizhou University of Commerce, Guiyang 550014, China
[3] School of Transportation Engineering, Guizhou Institute of Technology, Guiyang 550003, China; kangyirong@git.edu.cn
* Correspondence: gzysh2024@126.com or 202310957@gzcc.edu.cn

**Abstract:** This paper suggests a new multi-lane lattice model that incorporates both overtaking mechanisms and drivers' aggressive lane-changing behaviors to investigate macroscopic traffic stability in multi-lane expressway environments. To enhance the fidelity of lane-changing simulation, the proposed model reformulates lane-changing protocols by integrating empirical observations of aggressive driving patterns in real-world scenarios. Through theoretical derivation, we formulate a density wave partial differential equation that captures the spatio-temporal propagation of congestion patterns near critical stability thresholds while analytically obtaining the linear stability criterion for the proposed model. The validity of these theoretical constructs is validated through systematic numerical simulation. Key findings reveal that when overtaking passing rates are relatively low, the driver's aggressive lane-changing strategy exhibits a pronounced stabilizing effect on multi-lane systems and effectively mitigates traffic oscillation amplitudes. Conversely, under high passing rate conditions, such aggressive driving behaviors are shown to exert detrimental effects on both traffic fluctuation suppression and system-wide stability. Notably, our findings also demonstrate that expanding the number of lanes merges as a viable strategy to enhance systemic robustness.

**Keywords:** multi-lane lattice model; lane-changing rules; overtaking mechanism; nonlinear analysis; highways

**MSC:** 93D15

check for updates

Academic Editor: Aleksandr Rakhmangulov

Received: 25 February 2025
Revised: 4 April 2025
Accepted: 8 April 2025
Published: 15 April 2025

**Citation:** Yang, S.; Huang, B.; Tian, C.; Kang, Y. Modeling a Multi-Lane Highway System Considering the Combined Impacts of Overtaking Mechanisms and Aggressive Lane-Changing Behaviors. *Mathematics* **2025**, *13*, 1291. https://doi.org/10.3390/math13081291

**Copyright:** © 2025 by the authors. Licensee MDPI, Basel, Switzerland. This article is an open access article distributed under the terms and conditions of the Creative Commons Attribution (CC BY) license (https://creativecommons.org/licenses/by/4.0/).

## 1. Introduction

The issue of traffic congestion has emerged as an urgent societal challenge necessitating prompt attention to enhance transportation efficiency. To gain deeper insights into the underlying causes and dynamic progression of traffic congestion, researchers have devised and implemented a range of traffic flow models [1]. Recent advancements in this field encompass cellular automata models [2,3], car-following models [4,5], continuum models [6–8], and lattice models [9–11]. Collectively, these models can be classified into two major categories: microscopic traffic flow models and macroscopic traffic flow models. Microscopic traffic flow models focus on the perspective of individual vehicles, delving into the interactions between vehicles and their motion patterns. Macroscopic

traffic flow models, on the other hand, primarily concentrate on describing and analyzing the collective behavior of traffic flow. By treating traffic flow as a continuous fluid, these macroscopic models disregard the behavior of individual vehicles and instead emphasize the relationships among macroscopic variables such as traffic flux, velocity, and density. These models offer a robust framework for comprehending the multifaceted nature of traffic flow from diverse perspectives. Among these, the lattice model, initially proposed by Nagatani [9,10], has garnered significant academic interest due to its unique capability to concurrently capture both the macroscopic features and microscopic nuances of traffic flow. Consequently, several extended lattice models have been progressively introduced, incorporating novel influencing factors and mechanisms to better adapt to a wide array of traffic scenarios and the intricate, ever-changing traffic conditions. Table 1 presents the specifics of these extended lattice traffic flow models.

**Table 1.** Extensions and derivations of the lattice traffic flow model.

| Authors | Characteristics | References | Year | Scenario |
|---|---|---|---|---|
| Wang, Kaur, Kang, Zhai | Driver's predictive effect | [11–14] | 2019, 2020, 2024, 2023 | Highway |
| Redhu and Siwach | Traffic jerk | [15] | 2018 | Highway |
| Jin, Wang | Curved road with passing | [16,17] | 2019, 2017 | Highway |
| Peng and Kuang | Honk effect | [18,19] | 2019, 2019 | Highway |
| Wang, Ge, Qi | "Backward looking" effect | [20–22] | 2019, 2018, 2019 | Highway |
| Mei, Zhang, Jiang, Tian | On-ramp and off-ramp | [23–26] | 2021, 2018, 2019, 2025 | Highway |
| Long, Li | Flux limit effect | [27,28] | 2022, 2023 | Highway |
| Mei, Peng, Zhang | Self-stabilization effect | [23,29,30] | 2021, 2019, 2018 | Highway |
| Wang, Li, Zhai | Driver's memory effect | [31–34] | 2020, 2021, 2018, 2018 | Highway |
| Zhang, Peng, Pan, Zhao | Delayed-time effect | [35–38] | 2021, 2022, 2021, 2020 | Highway |
| Zhai and Wu | Cyber-attacks effect | [39] | 2021 | Highway |
| Sharma, Peng, Zhang | Driver's characteristics | [40–42] | 2016, 2019, 2015 | Highway |
| Peng, Redhu, Wang | Traffic interruption probability | [43–45] | 2018, 2015, 2019 | Highway |
| Zhu, Sun | Lane-changing rate | [46–48] | 2019, 2018, 2018 | Highway |
| Yang, Peng | Optimal flux difference estimation | [49,50] | 2016, 2018 | Highway |
| Tian, Peng | Optimal current difference | [51,52] | 2011, 2013 | Highway |
| Kang, Ge | Driver's physical delay | [53,54] | 2013, 2014 | Highway |

While traffic lattice models have received considerable academic scrutiny, prevailing research remains predominantly concentrated on single/double-lane configurations. This orientation sharply contrasts with real-world expressway architectures, which employ multi-lane operational systems (typically $\geq$3 lanes), yet limited attention has been directed toward developing comprehensive lattice-based analytical tools for such scenarios. Madaan and Sharma [55] broadened the modeling frontier by incorporating vehicle interaction governed by optimal velocity differentials, thereby bridging the methodological gap between conventional dual-lane theoretical constructs and practical application. Their subsequent investigation [56] systematically examined the role of temporal feedback mechanisms in multi-lane environments. The research trajectory culminated in Zhai et al.'s

2023 contribution [57], which formulated a high-fidelity hydrodynamic model taking into account overtaking dynamics. Empirical validation of these multi-lane analytical paradigms consistently demonstrates that integrating dynamic lane-switching protocols into system modeling can significantly enhance traffic dissipation mechanisms and flow optimization potential.

Lane changes are crucial in multi-lane traffic systems, as they enable vehicles to travel at their maximum speed and alleviate traffic congestion. As depicted in Figure 1, lane-changing behavior can occur between both adjacent and non-adjacent lanes, revealing that the operational complexity of lane-switching mechanisms in multi-lane configurations substantially exceeds dual-lane paradigms. Consequently, we anticipate that the dynamic properties of multi-lane systems will be significantly influenced by the lane-changing mechanism. Unfortunately, however, the current lane-changing assumptions [55–57] in multi-lane systems do not fully align with actual traffic operation patterns. Traditional lattice-based multi-lane models predominantly employ binary decision criteria comparing the vehicle headway (density-dependent) with the lateral distance to determine lane-switch feasibility. The governing heuristic typically postulates that a lane-switching event is initiated when lateral distance surpasses headway. However, this assumption is overly simplistic and fails to fully capture the complexities of real-world traffic. This lane-changing condition can lead to frequent and unnecessary lane changes, neglecting the required safety spacing constraints. In reality, drivers are often not sufficiently motivated to change lanes for such small differences between the vehicle headway and the lateral distance, especially when safety is a primary concern. Therefore, it is evident that the lane-switching mechanism in the current multi-lane framework needs to be systematically improved to better mimic real traffic scenarios.

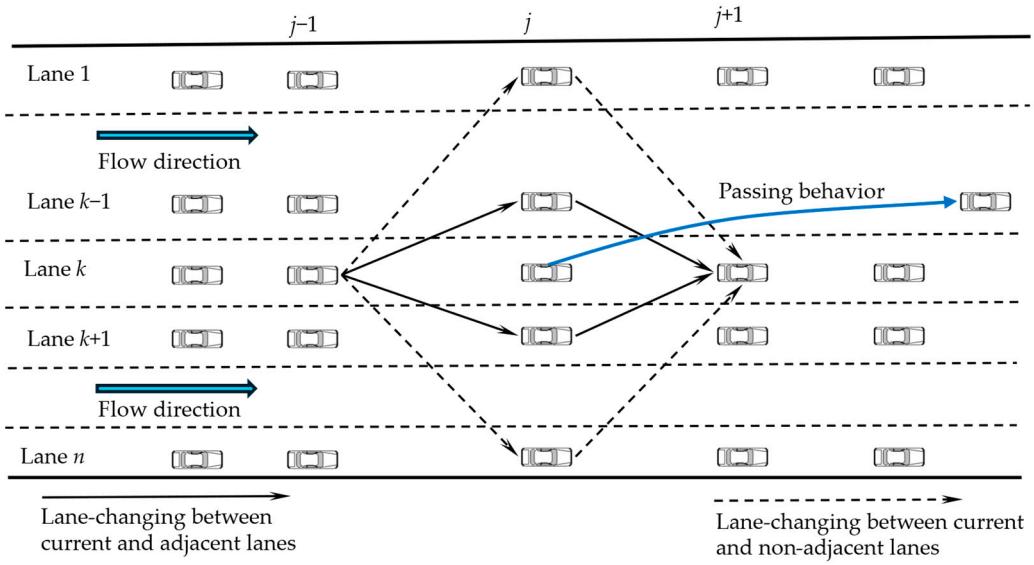



**Figure 1.** Visualization of typical vehicular interactions in multi-lane arterials highlighting lane-switching behaviors and overtaking maneuvers.

Moreover, as depicted in Figure 1, vehicles experiencing high traffic density on a highway typically exhibit passing behavior in addition to lane-changing. With the rapid development of Vehicle-to-Everything (V2X) technology, lane-changing and overtaking behaviors among vehicles in multi-lane systems will become more coordinated and intelligent, posing higher requirements for the construction of multi-lane system traffic flow models that accurately reflect actual traffic conditions. However, current multi-lane lattice models still fall short in capturing such coordinated features.

In summary, existing multi-lane lattice models demonstrate notable shortcomings in their lane-changing mechanisms. The current research landscape indicates that limited scholarly attention has been devoted to examining the synergistic effects of assertive lane-switching actions and overtaking maneuvers on emergent phenomena within multi-lane expressway environments. Addressing this critical knowledge void, our investigation establishes an enhanced multi-lane lattice model that holistically integrates overtaking mechanisms and assertive lane-switching tendencies within macroscopic traffic modeling paradigms. To enhance the realism of lane-changing rules, our new model reconstructs these rules based on aggressive lane-switching actions observed in real-world driving. Subsequently, we undertake comprehensive mathematical derivation and simulation experimentation. In real-world traffic contexts, the aim of the presented investigation is to systematically explore the combined effects of drivers' aggressive lane-changing and overtaking actions on traffic flow within multi-lane systems. Ultimately, the objective of this study lies in developing an analytical tool for simulating complex lane-dependent traffic phenomena, thereby elucidating the evolution patterns of multi-lane transportation systems.

The manuscript structure adheres to the following organization: Section 2 develops an N-lane lattice model through reformulated continuity equations and evolution equations, incorporating an enhanced lane-switching mechanism and passing effect. Sections 3 and 4 establish the analytical foundation through linear analysis and nonlinear wave dynamics investigation in the multi-lane system with passing, respectively. We derive the density wave partial equation that describes the propagation patterns of traffic jams in the multi-lane environments and the linear stability condition. Section 5 employs numerical simulations under cyclic boundary constraints to verify theoretical predictions about phase transition dynamics. Concluding remarks and future research directions are consolidated in the final section.

## 2. Models

Prior to examining operational principles of multi-lane highway systems, a concise overview of dual-lane traffic modeling methodology proves necessary. As illustrated in Figure 2, the two-lane system roadway is considered to consist of uniformly distributed discrete lattice points. In Figure 2, lane-changing behavior arises due to variable traffic volumes between the lattice locations on the two lanes, which results from drivers trying to drive more efficiently.

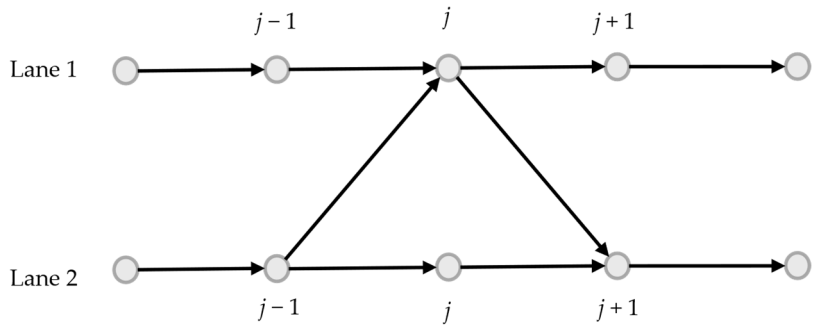



**Figure 2.** The schematic model of traffic flow on a two-lane highway [58].

Based on the lane-changing criteria proposed by Nagatani [10] for a two-lane system, when vehicular density at position $j-1$ on the secondary lane exceeds that at site $j$ on the primary lane, partial traffic flow transfers from lattice $j-1$ on lane 2 to lattice $j$ on lane 1 with switching coefficient $\gamma|\rho_0^2 V'(\rho_0)|\left(\rho_{2,j-1}-\rho_{1,j}\right)$. Conversely, when density at lane 1 (point $j$) surpasses that at lane 2 (point $j+1$), then the lane-changing rate from site $j$ on lane 1 to point

$j+1$ on lane 2 is $\gamma|\rho_0^2 V'(\rho_0)|(\rho_{1,j}-\rho_{2,j+1})$. Thus, for lane 1, this means that the total change brought by the lane-changing rate at lattice site $j$ is $\gamma|\rho_0^2 V'(\rho_0)|(\rho_{2,j-1}-2\rho_{1,j}+\rho_{2,j+1})$, In addition, since there is no inflow (source) or outflow (sink) of vehicles from ramps or other channels, the total number of vehicles remains conserved. Therefore, the continuity equation is expressed for lane 1 [10] as

$$\partial_t \rho_{1,j}(t)+\rho_0(\rho_{1,j}(t)v_{1,j}(t)-\rho_{1,j-1}(t)v_{1,j-1}(t))=\gamma|\rho_0^2 V'(\rho_0)|(\rho_{2,j-1}-2\rho_{1,j}+\rho_{2,j+1}) \quad (1)$$

Likewise, for lane 2:

$$\partial_t \rho_{2,j}(t)+\rho_0(\rho_{2,j}(t)v_{2,j}(t)-\rho_{2,j-1}(t)v_{2,j-1}(t))=\gamma|\rho_0^2 V'(\rho_0)|(\rho_{1,j-1}-2\rho_{2,j}+\rho_{1,j+1}) \quad (2)$$

where $\rho_{k,j}$ and $v_{k,j}$ denote the vehicular density and speed in lane k ($k$ = 1, 2) at position $j$.

Combining both equations yields the aggregated conservation equation for the dual-lane framework:

$$\partial_t \rho_j(t)+\rho_0\left(\rho_j(t)v_j(t)-\rho_{j-1}(t)v_{j-1}(t)\right)=\gamma|\rho_0^2 V'(\rho_0)|\left(\rho_{j+1}(t)-2\rho_j(t)+\rho_{j-1}(t)\right) \quad (3)$$

where $\rho_j=\left(\rho_{1,j}+\rho_{2,j}\right)/2$,$\rho_j v_j=\left(\rho_{1,j}v_{1,j}+\rho_{2,j}v_{2,j}\right)/2$. $\rho_j(t)$ and $v_j(t)$ denote the vehicular density and speed at the $j$th lattice at time $t$. $\rho_0$ signifies system-wide average density. The dimensionless scaling factor $\gamma|\rho_0^2 V'(\rho_0)|$ incorporates lane-switching coefficient $\gamma$ to maintain dimensional consistency in the conservation equations.

Additionally, it is assumed that the vehicles' lane changes have no bearing on the traffic flow's longitudinal motion process, and the motion equation is governed by [10]:

$$\rho_j(t+\tau)v_j(t+\tau)=\rho_0 V(\rho_{j+1}(t)) \quad (4)$$

$V(\rho)$ is the optimized velocity function, which is expressed as follows [10]:

$$V(\rho_j)=\tanh(\frac{2}{\rho_0}-\frac{\rho_j(t)}{\rho_0^2}-\frac{1}{\rho_c})+\tanh(\frac{1}{\rho_c}) \quad (5)$$

where $\rho_c$ is the critical density. As $\rho_0=\rho_c$, the optimized velocity function $V(\rho)$ has an inflection point at $\rho_j=\rho_c$.

Using V2X technology, drivers in the multi-lane system depicted in Figure 1 can obtain up-to-date traffic flow information about their surroundings. As a result, they are able to change lanes and pass not only between adjacent lanes but also across non-adjacent ones. In this multi-lane system, vehicles are free to switch between any of the n lanes. Given that each lane is homogeneous, the probability of a car selecting any lane is equal. For this multi-lane scenario, Madaan and Sharma developed a multi-lane lattice model in 2021 (hereinafter referred to as the MS multi-lane lattice model) and proposed the following assumptions during the modeling process [55]:

(1) For any designated lane k ($1 \leq$ k $\leq$ n), vehicular quantities remain preserved except for the lane-switching.
(2) When vehicular density at position $j-1$ in lane $k$ exceeds that at coordinate $j$ in target lane $m$ (m$\in$[1,n]; $m \neq k$), vehicles migrate from the $k$th to the $m$th lane with lane-switching rate $\gamma|\rho_0^2 V'(\rho_0)|(\rho_{k,j-1}-\rho_{m,j})$.
(3) Conversely, when vehicular density at position $j$ in lane m surpasses that at j+1 in lane k, inverse migration occurs with rate $\gamma|\rho_0^2 V'(\rho_0)|(\rho_{m,j}-\rho_{k,j+1})$.

These fundamental principles establish the vehicular conservation equation of the MS model for lane $k$ in multi-lane systems.

$$\partial_t \rho_{k,j} + \rho_0(\rho_{k,j} v_{k,j} - \rho_{k,j-1} v_{k,j-1}) = \gamma |\rho_0^2 V'(\rho_0)| \Big( \sum_{\substack{m=1 \\ m \neq k}}^{n} \rho_{m,j+1} + \sum_{\substack{m=1 \\ m \neq k}}^{n} \rho_{m,j-1} - 2(n-1)\rho_{k,j} \Big) \quad (6)$$

where $n$ denotes the total number of lanes of the roadway.

For analytical purposes, Madaan and Sharma further rewrote Equation (6) in the following form:

$$\partial_t \rho_j + \rho_0(\rho_j v_j - \rho_{j-1} v_{j-1}) = \gamma(n-1)|\rho_0^2 V'(\rho_0)|[\rho_{j-1} + \rho_{j+1} - 2\rho_j] \quad (7)$$

where $\rho_j = \frac{1}{n}\sum_{k=1}^{n} \rho_{k,j}$,$\rho_j v_j = \frac{1}{n}\sum_{k=1}^{n} \rho_{k,j} v_{k,j}$.

The evolution equation used in the MS multi-lane lattice model is formulated as

$$\rho_j(t+\tau) v_j(t+\tau) = \rho_0 V(\rho_{j+1}(t)) + \mu[\rho_0 V(\rho_{j+2}(t)) - \rho_0 V(\rho_{j+1}(t))] \quad (8)$$

where the expression $\rho_0 V\left(\rho_{j+2}(t)\right) - \rho_0 V\left(\rho_{j+1}(t)\right)$ represents the optimal current difference (OCD) on position $j$+1 at time $t$. The parameter $\mu$ serves as the sensitivity factor for OCD influence.

Nevertheless, the lane-switching threshold adopted in the conventional MS model and its derivatives demonstrates unrealistic characteristics. These models initiate lane shifting when minimal difference occurs between vehicle density at position $j-1$ in lane $k$ and site $j$ in adjacent lane $m$ ($m \neq k$). This constitutes an unrealistically proactive lane-shifting premise, particularly under high-density conditions where frequent lane transitions could compromise traffic safety. Empirical observations confirm that such intense lane-switching patterns rarely manifest in real-world congested scenarios, suggesting necessary modifications to both lane transition logic and associated continuity equations in multi-lane formulations.

Recently, Li et al. [59] have developed a more logical rule for lane changes in two-lane systems. This rule assumes that lane changes only happen when the available spacing in the target lane substantially exceeds their current headway by a defined multiplicative factor. Inspired by Li 's lane-changing mechanism design viewpoints, we reconstruct the lane-switching assumptions of the multi-lane lattice model in order to make it close to the traffic reality. Specifically, we propose that lane-changing behavior occurs at a rate governed by the rate $\gamma|\rho_0^2 V'(\rho_0)|\left(\rho_{k,j-1} - f\rho_{m,j}\right)$, activated when the density at position $j-1$ in lane $k$ surpasses $f$ times the density at cell $j$ in lane $m$. Here, $f$ quantifies the driver's propensity for lane-change maneuvers.

Similarly, when the vehicular density at lattice $j$ on lane $m$ exceeds by a factor $f$ the density at lattice $j$+1 on lane $k$, lane-switching will be activated with coefficient $\gamma|\rho_0^2 V'(\rho_0)|\left(\rho_{m,j} - f\rho_{k,j+1}\right)$. Implementing these revised lane-shifting criteria, the cumulative influx to lattice $j$ on lane $k$ from lattice $j$-1 on adjacent lane $m$ (m $\neq$ k) can be expressed as $\sum_{\substack{m=1 \\ m \neq r}}^{n} \gamma|\rho_0^2 V'(\rho_0)|\left(\rho_{m,j-1} - f\rho_{r,j}\right)$. Conversely, the total outflow from lattice $j$ on lane $k$ to lattice $j$+1 on other lanes is quantified by $\sum_{\substack{m=1 \\ m \neq r}}^{n} \gamma|\rho_0^2 V'(\rho_0)|\left(\rho_{r,j} - f\rho_{m,j+1}\right)$. Consequently, the net density variation at cell $j$ on lane $k$ induced by lane transfers becomes $\gamma\left|\rho_0^2 V'(\rho_0)\right|\sum_{\substack{m=1 \\ m \neq r}}^{n}\left(\rho_{m,j-1}\right) - (n-1)(f+1)\rho_{r,j} + f\sum_{\substack{m=1 \\ m \neq r}}^{n}\left(\rho_{m,j+1}\right)$. These considerations yield the general continuity equation for the $k^{th}$ lane in a multi-lane expressway system:

$$\partial_t \rho_{k,j} + \rho_0(\rho_{k,j} v_{r,j} - \rho_{k,j-1} v_{k,j-1}) = \gamma|\rho_0^2 V'(\rho_0)| \left( \sum_{\substack{m=1 \\ m \neq k}}^{n} \rho_{m,j-1} + f \sum_{\substack{m=1 \\ m \neq k}}^{n} \rho_{m,j+1} - (f+1)(n-1)\rho_{k,j} \right) \quad (9)$$

Through aggregation of all lane-specific information from Equation (9), the macroscopic continuity equation for the multi-lane system emerges as

$$\partial_t \rho_j + \rho_0(\rho_j v_j - \rho_{j-1} v_{j-1}) = \gamma(n-1)\left|\rho_0^2 V'(\rho_0)\right|[\rho_{j-1} + f\rho_{j+1} - (f+1)\rho_j] \tag{10}$$

It is important to emphasize that in a multi-lane system, the lateral distance and headway of the vehicle in question are crucial factors influencing the driver's lane-changing decision. The ratio $f$, which represents the relationship between these two distances, directly reflects the driver's level of aggressiveness when changing lanes. Specifically, given a certain vehicle density (or headway) in the current lane, a smaller value of $f$ indicates a higher density in the target lane, suggesting that the driver requires less lateral space to execute the lane change and thus demonstrates a more aggressive driving style. Conversely, a larger value of $f$ indicates that the driver is more cautious and conservative when changing lanes. Therefore, the parameter $f$ serves as a reliable indicator for measuring the level of aggressiveness in lane-changing behavior within a multi-lane framework, with the driver's level of aggressiveness being inversely proportional to this value.

Furthermore, passing behavior is a common phenomenon in multi-lane systems on highways. It has been extensively studied in single-lane and two-lane lattice model scenarios [16,17,40]. However, the passing effect has been less studied within multi-lane systems [57]. Obviously, while reconstructing the lane-changing mechanism, we further introduce the passing effect into the traffic flow evolution equation, which will effectively improve the simulation accuracy and capability of the multi-lane lattice model. In fact, according to the literature [16,17,40,57], passing behavior occurs when the flow on a lattice site $j$ exceeds the flow on the lattice site $j+1$ in front of it, and the amount of passing on the lattice site $j$ is proportional to the difference between the optimal flow on the lattice point $j$ and on the lattice point $j$+1. Consequently, the evolution equation for the highway multi-lane lattice model can be improved as follows:

$$\rho_j(t+\tau)v_j(t+\tau) = \rho_0 V(\rho_{j+1}(t)) + \lambda[\rho_0 V(\rho_{j+1}(t)) - \rho_0 V(\rho_{j+2}(t))] \tag{11}$$

where $\Delta F = \rho_0 V(\rho_{j+1}(t)) - \rho_0 V(\rho_{j+2}(t))$ is the optimal flow difference generated by the overtaking factor and $\lambda$ is the corresponding passing constant.

At this point, we now develop an enhanced multi-lane lattice model comprising Equations (10) and (11), which accounts for the impacts of aggressive lane-shifting and overtaking behaviors. When $f = 1$, our generalized model reduces to Zhai's model [57]. While further imposing $\lambda = 0$ yields the MS model, which demonstrates that the MS model exists as a particular instance within our expanded modeling paradigm.

Through systematic elimination of the speed parameters in Equations (10) and (11), we derive the density evolution equation governing multi-lane traffic systems:

$$\begin{aligned}&\rho_j(t+2\tau) - \rho_j(t+\tau) + \tau\rho_0^2[(V(\rho_{j+1}(t)) - V(\rho_j(t)))] + \lambda\tau\rho_0^2[2V(\rho_{j+1}(t)) - V(\rho_j(t))\\ &-V(\rho_{j+2}(t))] - \gamma(n-1)\tau\left|\rho_0^2 V'(\rho_0)\right|[\rho_{j-1}(t+\tau) + f\rho_{j+1}(t+\tau) - (f+1)\rho_j(t+\tau)] = 0\end{aligned} \tag{12}$$

## 3. Linear Stability Analysis

When the traffic density at all lattice sites on the roadway is uniformly maintained as $\rho_0$, with a corresponding steady-state velocity distribution $V(\rho_0)$, the traffic flow evidently attains a steady-state distribution. Under this condition, $\rho_j(t+\tau) = \rho_j(t) = \rho_0$, $v_j(t+\tau) = v_j(t) = V(\rho_0)$ holds true. Based on this equilibrium state, it can be derived that $\partial_t \rho_j = 0$ in

Equations (10) and (11) is satisfied. Therefore, the steady-state solution of the density evolution Equation (12) for the multi-lane highway system is given by

$$\rho_j(t) = \rho_0,\ v_j(t) = V(\rho_0) \tag{13}$$

Applying a small perturbation signal $y_j(t)$ to the steady-state solution, we obtain

$$\rho_j(t) = \rho_0 + y_j(t) \tag{14}$$

Substituting Equation (14) into Equation (12) and linearizing the equation, the following can be obtained:

$$\begin{aligned} &y_j(t+2\tau) - y_j(t+\tau) + \tau\rho_0^2 V'(\rho_0)[y_{j+1}(t) - y_j(t)] + \lambda\tau\rho_0^2 V'(\rho_0)[2y_{j+1}(t) \\ &-y_j(t) - y_{j+2}(t)] - (n-1)\tau\gamma\left|\rho_0^2 V'(\rho_0)\right|[\rho_{j-1}(t+\tau) \\ &+f\rho_{j+1}(t+\tau) - (f+1)\rho_j(t+\tau)] = 0 \end{aligned} \tag{15}$$

where $V'(\rho_0) = [dV(\rho_j)/d\rho_j]\big|_{\rho_j=\rho_0}$. Expanding $y_j(t)$ in Equation (15) as a Fourier series form, $y_j(t) = \exp(ikj + zt)$, one can obtain

$$\begin{aligned} &e^{2\tau z} - e^{\tau z} + \tau\rho_0^2 V'(\rho_0)(e^{ik} - 1) + \lambda\tau\rho_0^2 V'(\rho_0)(2e^{ik} - 1 - e^{2ik}) \\ &-(n-1)\tau\gamma\left|\rho_0^2 V'(\rho_0)\right|(e^{-ik} + (f+1) + fe^{ik}) = 0 \end{aligned} \tag{16}$$

Expanding the parameter $z$ in Equation (16) into the form $z = z_1 ik + z_2 (ik)^2 + \cdots$ and then retaining the first-order and second-order terms with respect to $ik$, one can obtain

$$z_1 = -\rho_0^2 V'(\rho_0) + (n-1)(f-1)\gamma\left|\rho_0^2 V'(\rho_0)\right| \tag{17}$$

$$z_2 = -\frac{3\tau z_1^2}{2} - \frac{\rho_0^2}{2}V'(\rho_0) + \lambda\rho_0^2 V'(\rho_0) + \frac{1}{2}\gamma(1+f)(n-1)\left|\rho_0^2 V'(\rho_0)\right| \tag{18}$$

According to the judgment criterion of the long-wave expansion method, when $z_2 < 0$, the traffic system becomes unstable. In this scenario, the small perturbation signal grows and intensifies within the traffic flow as time progresses. Conversely, when $z_2 > 0$, the traffic system maintains its stability. Under these circumstances, the small perturbation signal gradually diminishes over time, and the traffic flow ultimately converges to a steady state. Consequently, we can deduce the critical stability conditions for the novel model as detailed below:

$$\tau = -\frac{1 - 2\lambda + (1+f)(n-1)\gamma}{3[1 + (n+1)(f-1)\gamma]\rho_0^2 V'(\rho_0)} \tag{19}$$

The criterion for maintaining stability in the multi-lane traffic lattice model is

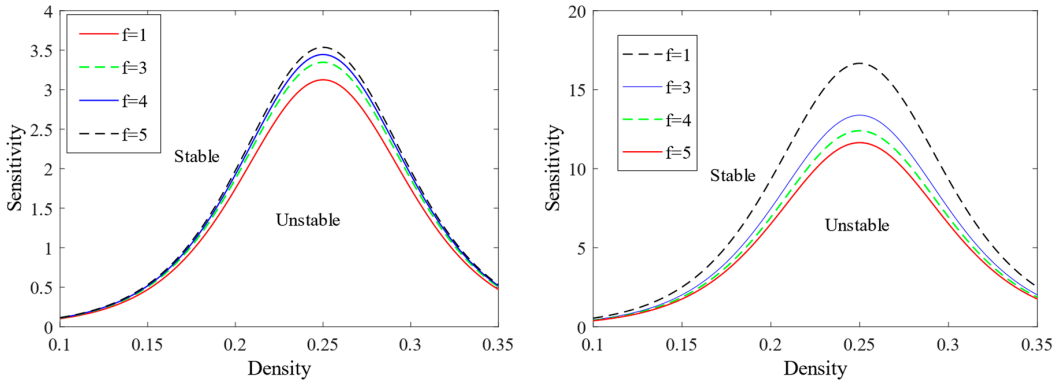
$$\tau < -\frac{1 - 2\lambda + (1+f)(n-1)\gamma}{3[1 + (n+1)(f-1)\gamma]\rho_0^2 V'(\rho_0)} \tag{20}$$

In particular, when $f = 1$, the stability conditions obtained by the new model are consistent with Zhai's model [57], as follows:

$$\tau < -\frac{1 - 2\lambda + 2(n-1)\gamma}{3\rho_0^2 V'(\rho_0)} \tag{21}$$

The stability condition (20) of our new model clearly reveals the pivotal roles of the overtaking passing rate constant $\gamma$ and the lane change adjustment intensity coefficient (LCAIC) $f$ in determining the stability of multi-lane systems. When $n = 3$ and $\gamma = 0.02$. Figure 3 illustrates the critical stability curves of our model in the phase space $(\rho, a)$,

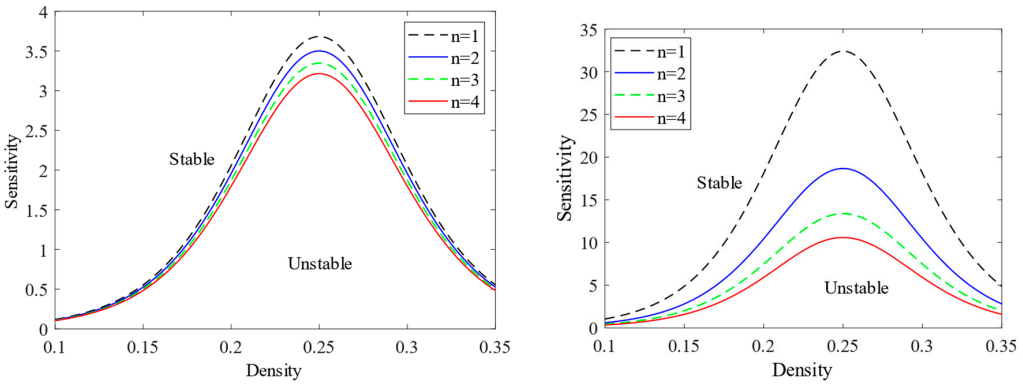
presenting two scenarios of overtaking passing rates associated with different values of $f$. Specifically, Figure 3a portrays a situation with a low overtaking passing rate ($\lambda = 0.06$), whereas Figure 3b illustrates a scenario with a high one ($\lambda = 0.45$). In these figures, each critical stability curve divides the phase space into two distinct zones: the area below the curve denotes instability, while the region above signifies stability. A key highlight on these curves is the presence of a critical point. A comparison of Figure 3a,b highlights that the parameter $f$ exerts a markedly different influence on the overall traffic stability of the multi-lane system, dependent on the overtaking passing rate constant. In instances where this constant $\gamma$ is small, as seen in Figure 3a, an increase in $f$ leads to a gradual reduction in the stability region, suggesting a decline in the system's traffic stability. On the other hand, when the overtaking passing rate constant $\gamma$ is large, as depicted in Figure 3b, an elevation in $f$ enhances the stability of traffic flow.




(**a**) $\lambda = 0.06$ (**b**) $\lambda = 0.45$

**Figure 3.** The neutral stability curves for the presented model in density–sensitivity space with a different parameter $f$, where subplots (**a**,**b**) correspond to the cases for $\lambda = 0.06$ and $\lambda = 0.45$, respectively.

Figure 4 shows the critical stability curves of the new model in phase space $(\rho, a)$ for the parameter $f = 3$, $\gamma = 0.02$, corresponding to different numbers of lanes $n$. Figures 4a and 4b correspond to the cases where the overtaking passing rate constants are 0.06 and 0.45, respectively. From Figure 4, we can clearly see that the critical stability curves of the proposed model gradually decrease with the increase in the number of lanes of the multi-lane system, regardless of whether the overtaking passing rate is low or relatively high. This indicates that the traffic stability of the multi-lane system gradually increases with the number of lanes. This finding highlights the positive effect of the number of lanes on traffic stability in multi-lane systems.




(**a**) $\lambda = 0.06$ (**b**) $\lambda = 0.45$

**Figure 4.** The neutral stability curves for the presented model in density–sensitivity space with different $n$, where the subplots (**a**,**b**) correspond to the cases for $\lambda = 0.06$ and $\lambda = 0.45$, respectively.

## 4. Nonlinear Analysis

In this section, we make use of nonlinear analytical methods to study the propagation evolution mechanism of the traffic congestion near the critical stable point $(\rho_c, a_c)$ of the multi-lane highway system. For this purpose, we define the slow variables $X$ and $T$ as follows:

$$X = \varepsilon(j + bt),\ T = \varepsilon^3 t,\ 0 < \varepsilon \leq 1 \tag{22}$$

where the parameters $j$ and $t$ represent spatial and temporal variables, respectively. The parameter $b$ is the coefficient to be determined. We further assume that the density variable satisfies

$$\rho_j(t) = \rho_c + \varepsilon R(X, T) \tag{23}$$

Bringing Equations (22) and (23) to the density evolution Equation (12) and performing a Taylor expansion up to the order of $\varepsilon^5$, we obtain the following partial differential equation (Refer to Appendix A for details):

$$\begin{array}{l}\varepsilon^2[b + \rho_c^2 V' + \gamma(n-1)(f-1)\rho_c^2 V']\partial_X R + \varepsilon^3\{\frac{3}{2}b^2\tau + \frac{1-\lambda}{2}\rho_c^2 V' \\ + \frac{\gamma(n-1)[1-2b\tau+f(1+2b\tau)]}{2}\rho_c^2 V'\}\partial_X^2 R + \varepsilon^4\{\partial_T R + [\frac{7b^3\tau^2}{6} + \frac{1-6\lambda}{6}\rho_c^2 V' \\ + \frac{\gamma(n-1)(3b^2\tau^2(f-1)+3b\tau(1+f)+f-1)}{6}\rho_c^2 V']\partial_X^3 R + \frac{\rho_c^2 V'''}{6}\partial_X R^3\} \\ + \varepsilon^5\{[3b\tau + \gamma\tau(n-1)(f-1)\rho_c^2 V']\partial_X\partial_T R + [\frac{5b^4\tau^3}{8} + \frac{1-14}{24}\rho_c^2 V' \\ + \frac{\gamma(n-1)[(4b^3\tau^3+4b\tau)(f-1)+(6b^2\tau^2+1)(f+1)]}{24}\rho_c^2 V']\partial_X^4 R \\ + \frac{1-2\lambda}{12}\rho_c^2 V'''\partial_X^2 R^3\} = 0\end{array} \tag{24}$$

where $V' = [\frac{dV(\rho_j)}{d\rho_j}]|\rho_j = \rho_c$ and $V''' = [\frac{d^3V(\rho_j)}{d\rho_j^3}]|\rho_j = \rho_c$. At the critical point $(\rho_c, a_c)$, let $\tau = (1 + \varepsilon^2)\tau_c$, and $b = -\rho_c^2 V' - \gamma(n-1)(f-1)\rho_c^2 V'$, then the second- and third-order terms of $\varepsilon$ in Equation (24) can be eliminated, resulting in the following simplified equation:

$$\varepsilon^4[\partial_T R - g_1\partial_X^3 R + g_2\partial_X R^3] + \varepsilon^5[g_3\partial_X^2 R + g_4\partial_X^4 R + g_5\partial_X^2 R^3] = 0 \tag{25}$$

where

$$\begin{array}{l}g_1 = -\Big[\frac{7b^3\tau_c^2}{6} + \frac{1-6\lambda}{6}\rho_c^2 V' + \frac{\gamma(n-1)\left(3b^2\tau_c^2(f-1)+3b\tau_c(1+f)+f-1\right)}{6}\rho_c^2 V'\Big], g_2 = \frac{\rho_c^2 V'''}{6} \\ g_3 = \frac{3b^2\tau_c+2\gamma(n-1)(f-1)b\tau_c\rho_c^2 V'}{2} \\ g_4 = -\left[3b\tau_c + \gamma\tau(n-1)(f-1)\rho_c^2 V'\right]\Big[\frac{7b^3\tau_c^2}{6} + \frac{1-6\lambda}{6}\rho_c^2 V' + \frac{5b^4\tau_c^3}{8} + \frac{1-14}{24}\rho_c^2 V' + \\ \frac{\gamma(n-1)\left(3b^2\tau_c^2(f-1)+3b\tau_c(1+f)+f-1\right)}{6}\rho_c^2 V'\Big] + \frac{\gamma(n-1)\left[\left(4b^3\tau_c^3+4b\tau_c\right)(f-1)+\left(6b^2\tau_c^2+1\right)(f+1)\right]}{24}\rho_c^2 V'\Big] \\ g_5 = \frac{1-2\lambda-2\left[3b\tau_c+\gamma\tau_c(n-1)(f-1)\rho_c^2 V'\right]}{12}\rho_c^2 V'''\end{array}$$

To derive the standard mKdV equation, the following mathematical transformations are introduced:

$$T' = g_1 T,\ R = \sqrt{\frac{g_1}{g_2}}R' \tag{26}$$

Based on Equation (26), we can change Equation (25) into the following form:

$$\partial_{T'} R' - \partial_X^3 R' + \partial_X R'^3 + \varepsilon M[R'] = 0 \tag{27}$$

where

$$M[R'] = \frac{1}{g_1}[g_3\partial_X^2 R' + g_4\partial_X^4 R' + \frac{g_1 g_5}{g_2}\partial_X^2 R'^3] \tag{28}$$

By ignoring the correction term $M[R']$ in Equation (27), we derive the standard mKdV equation that corresponds to the proposed multi-lane lattice model (12). Furthermore, we

find the solution to this mKdV equation, yielding the associated kink–antikink soliton wave solution, which is expressed as

$$R'_0(X, T') = \sqrt{c}\tanh\sqrt{\frac{c}{2}}(X - cT') \tag{29}$$

where the parameter $c$ denotes the speed of propagation of the traffic flow density wave. To ascertain the value of $c$, the following conditions must be met:

$$(R'_0, M[R'_0]) = \int_{-\infty}^{+\infty} dX R'_0(X, T') M[R'_0(X, T')] = 0 \tag{30}$$

Based on Equation (30), the following calculation formula for the parameter $c$ can be obtained [60]:

$$c = 5g_2g_3/(2g_2g_4 - 3g_1g_5) \tag{31}$$

At this stage, we can derive the kink–antikink density wave solution for the mKdV equation as follows:

$$\rho_j(t) = \rho_c + \sqrt{\frac{g_1c}{g_2}(\frac{\tau}{\tau_c} - 1)}\tanh\sqrt{\frac{c}{2}(\frac{\tau}{\tau_c} - 1)}[j + (1 - cg_1(\frac{\tau}{\tau_c} - 1))t] \tag{32}$$

The corresponding amplitude $A$ can be calculated using the formula

$$A = \sqrt{\frac{g_1c}{g_2}(\frac{\tau}{\tau_c} - 1)} \tag{33}$$

The kink–antikink wave solution represents the coexistence phase in traffic flow, characterized by the simultaneous presence of the free-flow phase (for low-density traffic) and the congestion phase (for high-density traffic) within a multi-lane system. During this coexistence phase, traffic in the multi-lane system rapidly oscillates between the free-flow and congested phases, creating a structure analogous to a kink–antikink pair. This typical traffic flow pattern is clearly evident in Section 5, and it closely matches the theoretical predictions obtained from the nonlinear analysis presented in this section. As a result, the evolution of traffic flow under the combined influence of drivers' aggressive lane-changing behavior and overtaking mechanisms in a multi-lane setting can be accurately modeled by the mKdV equation and its associated kink–antikink wave solution, as derived in this section.

## 5. Numerical Simulation

In this section, we conduct numerical simulation experiments with periodic boundary conditions to verify the accuracy of the preceding theoretical analysis. The simulation setup is as follows: A circular lane is evenly divided into 100 grid cells. Initially, vehicles are evenly distributed along the road and maintain a constant speed. To assess the model's dynamic behavior in response to external disturbances, we introduce slight disturbance signals to the traffic flow in two sections of the road at the outset. The detailed initial conditions are given below: $\rho_j(0) = \rho_0 = 0.25$, $\rho_j(1) = \rho_j(0) = 0.25$, $j \neq 50, 51$, $\rho_j(1) = 0.25 - 0.1$ ($j = 50$), and $\rho_j(1) = 0.25 + 0.1$ ($j = 51$). The other simulation input parameters are set as follows: total number of road cells $N = 100$ and lane-changing rate $\gamma = 0.02$. The simulation results are illustrated in Figures 5–16.

Figure 5 depicts the three-dimensional evolution of traffic density for the proposed model across different lane counts $n$ under low overtaking passing rates ($\lambda = 0.06$), with the input parameters set at $a = 3.1$ and $f = 3$. The figure indicates that, due to the violation of the stability condition (20), perturbation signals amplify during vehicle interactions,

ultimately leading to traffic congestion. This congestion propagates upstream in the traffic flow in the form of kink–antikink waves. However, it is noteworthy that the extent of traffic congestion decreases as the number of lanes increases.

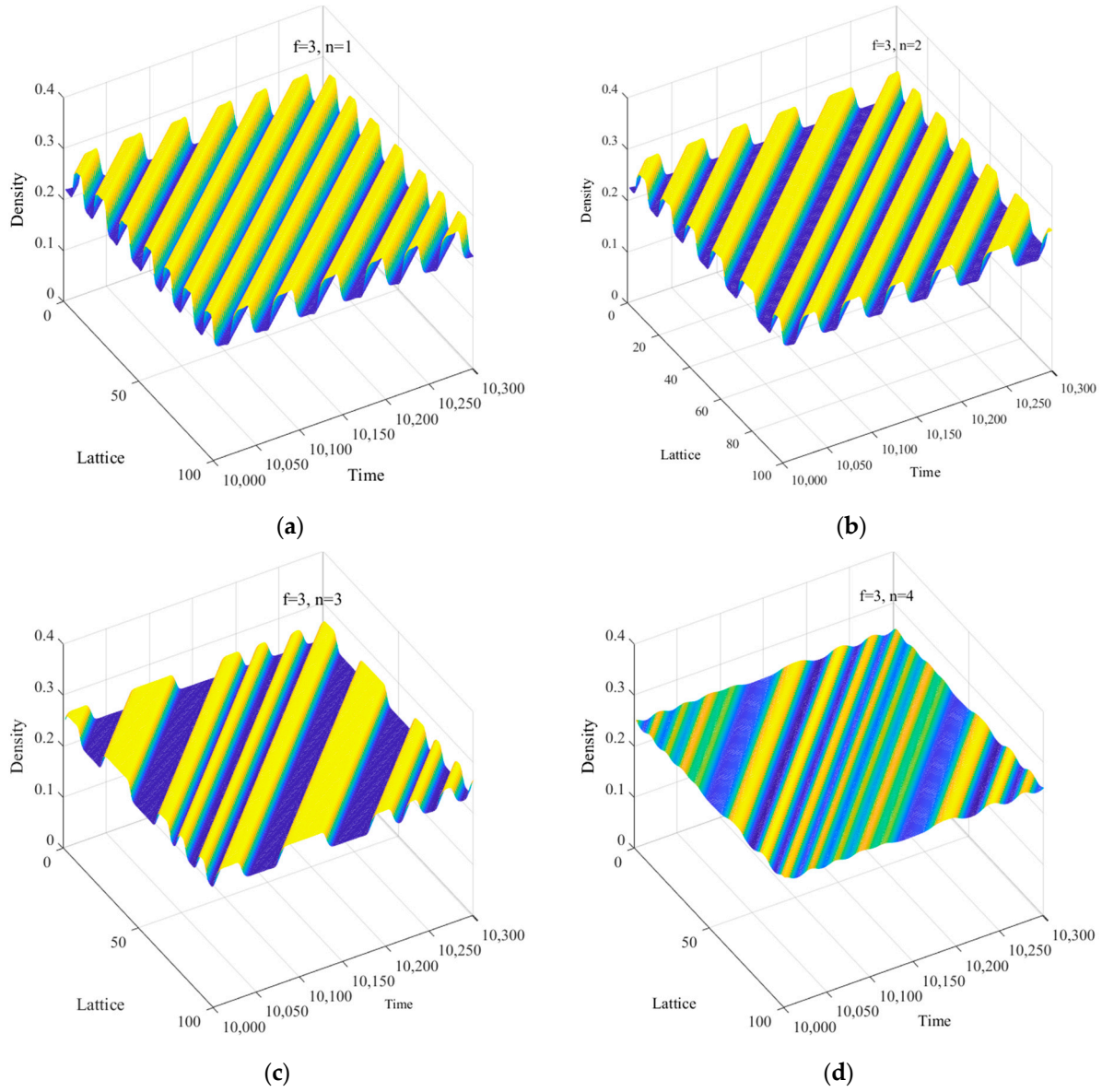



**Figure 5.** Space–time evolution of the density after t = 10,000 with $a = 3.1$, $f = 3$. The patterns (**a**), (**b**), (**c**), and (**d**) with $\lambda = 0.06$ are for $n = 1,\ 2,\ 3,\ 4$, respectively.

To more clearly illustrate the beneficial impact of increasing the number of lanes on reducing traffic congestion, Figure 6 displays the traffic density distribution across all grid points (road segments) at the time step t = 10,300. The figure reveals that as the number of lanes $n$ increases, the amplitude of the kink–antikink wave fluctuations notably diminishes, and the frequency of these fluctuations also progressively decreases. This provides compelling evidence that the stability of the traffic flow has been significantly enhanced.

When the overtaking passing rate is high ($\lambda = 0.45$), Figure 7 demonstrates the spatio-temporal evolution of the traffic density for the present model with different numbers of lanes. Additionally, Figure 8 presents the distribution of traffic density at all grid point locations at time step t = 10,300, corresponding to the scenarios depicted in Figure 7. By comparing Figures 7 and 8 with the previous Figures 5 and 6, we can draw a similar conclusion: the traffic stability of the multi-lane system increases with the number of lanes,

irrespective of the overtaking passing rate. This finding closely aligns with the conclusions of the linear stability analysis presented in Figure 4, further confirming the positive impact of the number of lanes on the smoothness and stability of traffic flow operations.

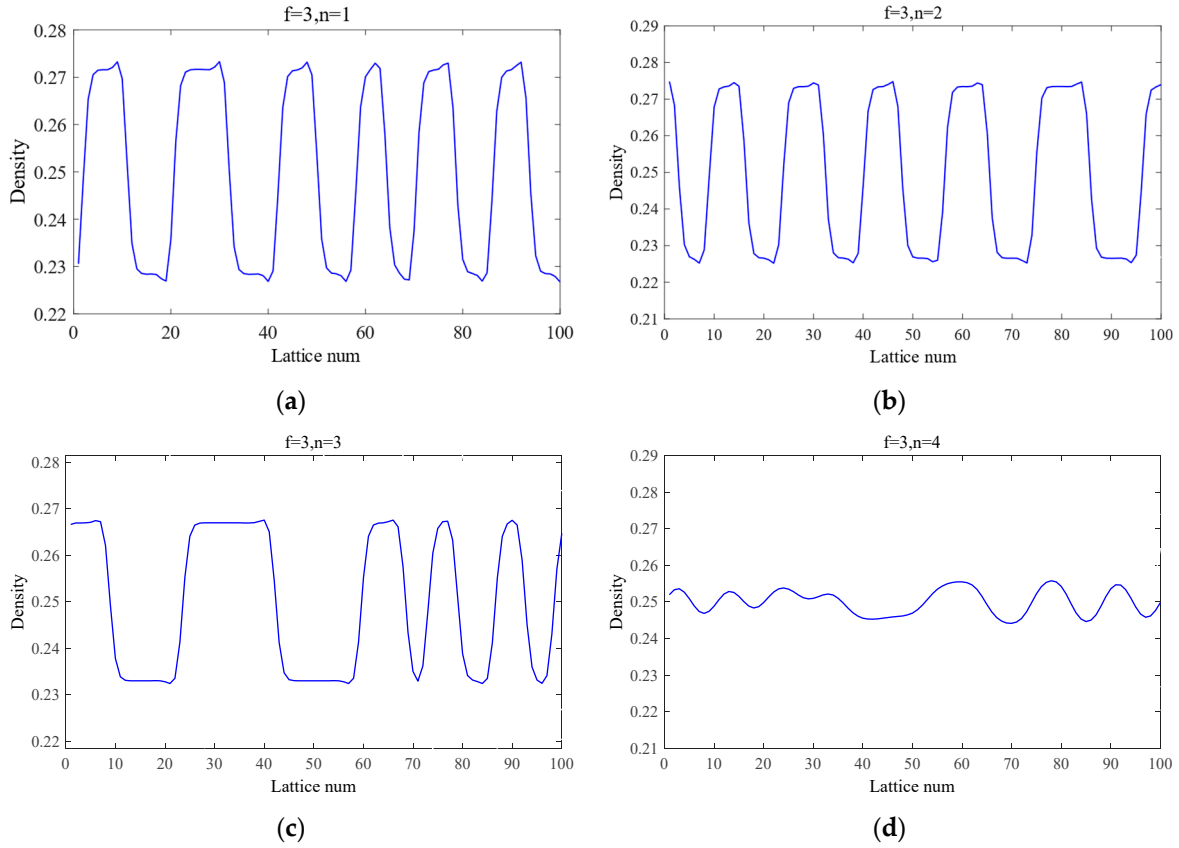



**Figure 6.** (**a**–**d**) Density profiles of the density wave at t = 10,300 correspond to the panels in Figure 5.

Figure 9 depicts in detail the three-dimensional distribution of the traffic density of this new model at various values of $f$ after sufficient evolution when the overtaking rate is low ($\lambda = 0.06$). In Figure 9a, the LCAIC parameter $f = 1$, at which the system evolution coincides with Zhai's model [57], shows that the traffic flow gradually returns to a uniformly distributed free-flow state when the stability condition (20) is satisfied, and the small perturbation signals are completely absorbed by the system over time. However, when the LCAIC parameter $f$ takes values of 3, 4, and 5 (as shown in Figure 9b–d), the multi-lane system begins to exhibit signs of traffic congestion as the stability condition (20) is no longer satisfied. In order to more concretely show the effect of drivers' aggressive lane-changing behavior on the stability of the multi-lane system, corresponding to Figure 9, Figure 10 provides a profile of the traffic density distribution at all grid points at the time step t = 10,300. Figure 10 demonstrates in a more visual way the significant effect of drivers' aggressive lane-changing strategies on alleviating traffic congestion when the overtaking passing rate is low. In this case, the driver can actively avoid the congestion ahead of the current lane by adopting an aggressive lane-changing strategy, thereby enabling the multi-lane system to operate in a more optimal state.

Figure 11 demonstrates the spatio-temporal evolution of traffic density for the present model, corresponding to different values of $f$, after the system has fully evolved in the case of a high overtaking rate ($\lambda = 0.45$). Corresponding to Figure 11, Figure 12 further displays the traffic density distribution at all grid points at the time step t = 10,300. From these two figures, we observe a clear trend: as the degree of aggressive lane-changing increases (i.e., as the LCAIC f-value decreases), the stability of the multi-lane system gradually decreases,

and the magnitude of traffic congestion fluctuations gradually increases. This phenomenon can be explained by the fact that in a multi-lane system with a high overtaking frequency, if drivers frequently adopt aggressive lane-changing strategies, these lane changes, when superimposed with overtaking behaviors, exacerbate the disorder of the system and ultimately lead to the frequent emergence and worsening of traffic congestion. This finding aligns with our observations of real-world traffic.

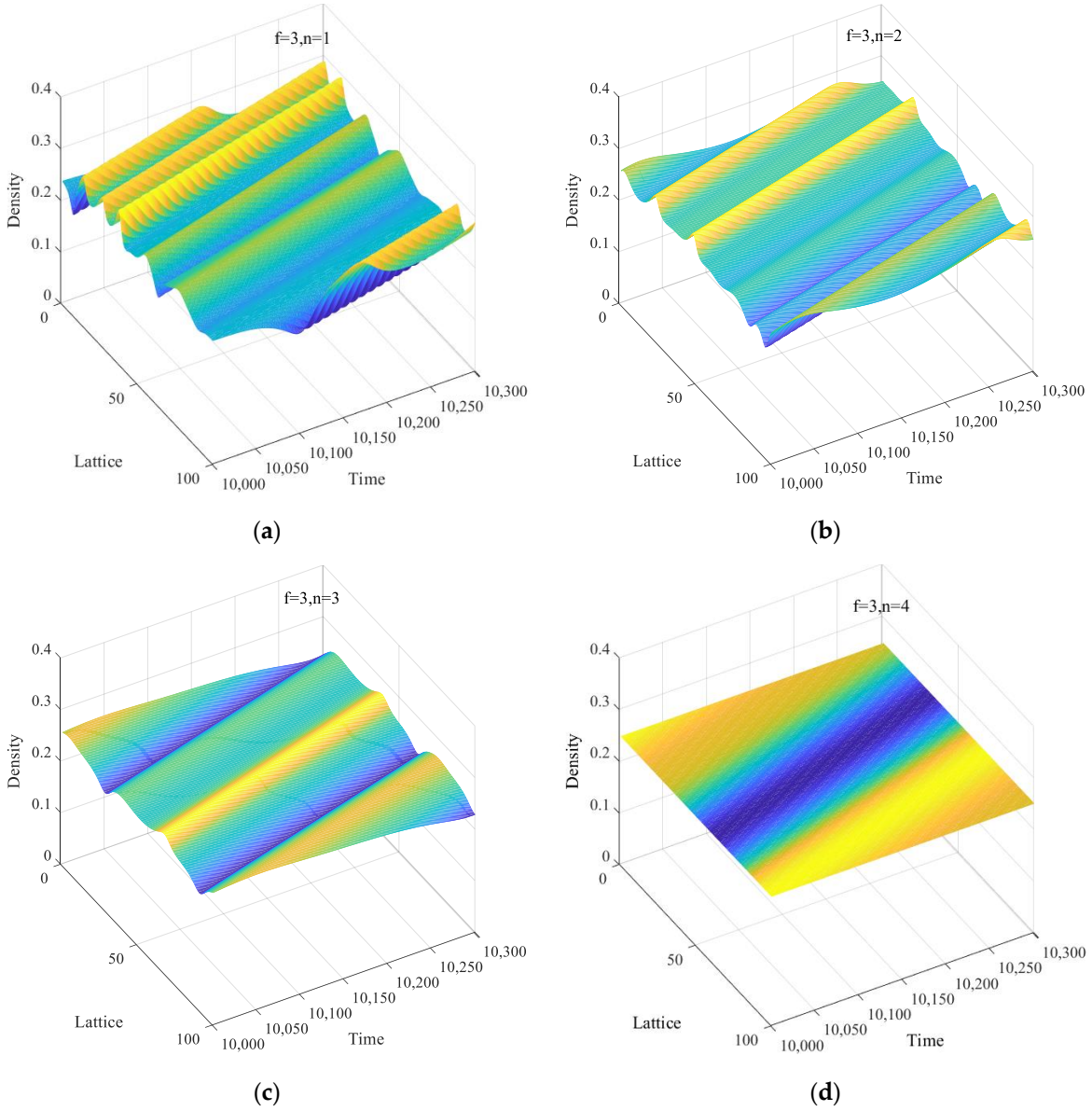



**Figure 7.** Space–time evolution of the density after t = 10,000 with $a = 11$, $f = 3$. The patterns (**a**), (**b**), (**c**), and (**d**) with $\lambda = 0.45$ are for $n = 1,\ 2,\ 3,\ 4$, respectively.

By comparatively analyzing the patterns observed in the two cases of low overtaking rate (as shown in Figures 9 and 10) and high overtaking rate (as shown in Figures 11 and 12), we can clearly observe that different combinations of the overtaking rate and the driver's aggressive lane-changing behavior have distinctly different effects on the stability of the multi-lane system. Specifically, when the overtaking rate is low, the driver's aggressive lane-changing behavior actually has a positive impact on the stability of the multi-lane system. However, once the overtaking rate rises to a high level, the driver's aggressive lane-changing behavior becomes a detrimental factor to the system's stability, and the stability of the system gradually decreases as the degree of the driver's aggressive lane-changing

increases. It is worth noting that this simulation result fully corroborates the accuracy of the linear stability theory analysis presented in Figure 3. The aforementioned conclusions were obtained under a lane-changing rate of $\gamma = 0.02$. To examine whether similar conclusions can be drawn under higher lane-changing rate conditions, we present traffic density evolution diagrams corresponding to different parameter $f$ values for two scenarios: low overtaking rate ($\lambda = 0.06$) and high overtaking rate ($\lambda = 0.45$) at $\gamma = 0.1$, as illustrated in Figures 13 and 14.

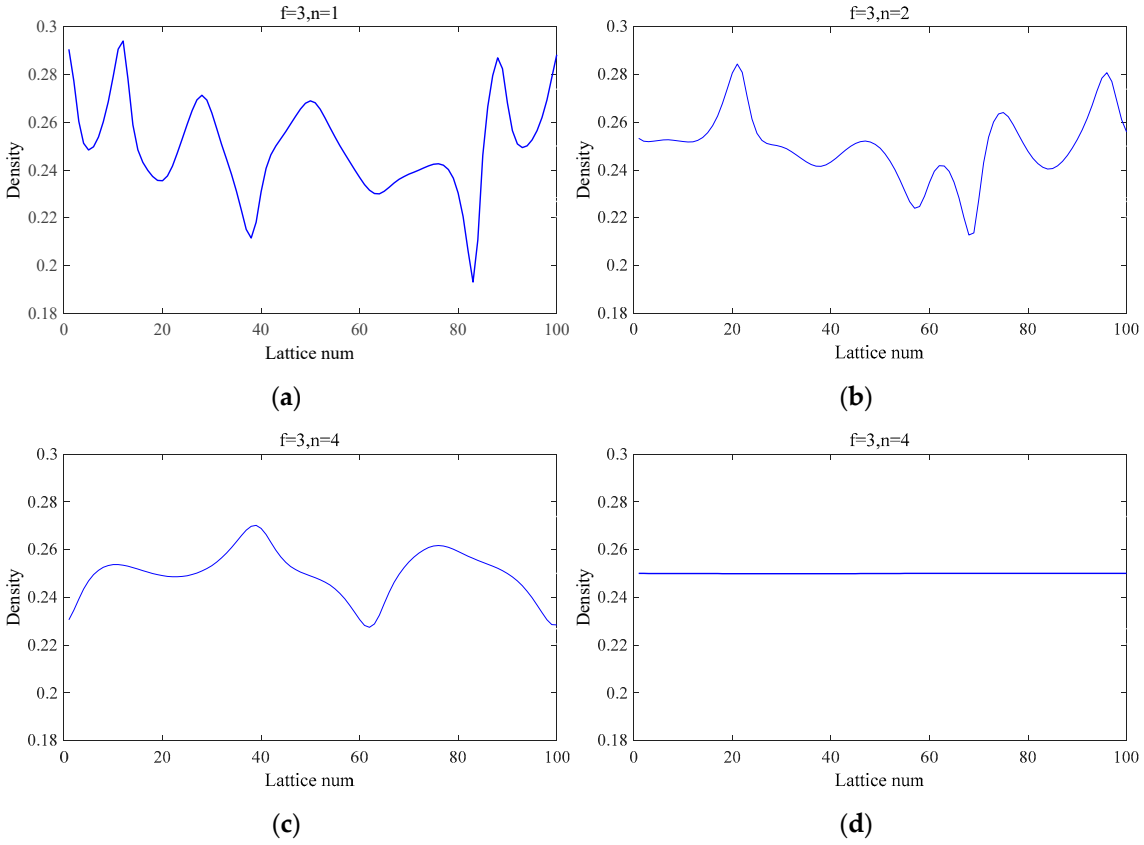



**Figure 8.** (**a**–**d**) Density profiles of the density wave at t = 10,300 correspond to the panels in Figure 7.

Figure 13 illustrates traffic density distributions under low overtaking rate conditions with lane-changing rate $\gamma = 0.1$ for different parameter $f$ values. Subfigures (a) and (b) display profiles of the density wave at $t = 200$ and $t = 10300$. Figure 14 presents the corresponding traffic density evolution patterns under high overtaking rate conditions. From Figure 13, it can be observed that when the overtaking rate is low ($\lambda = 0.06$), the stability of multi-lane traffic flow strengthens as parameter f decreases. However, Figure 14 reveals that under high overtaking rate conditions ($\lambda = 0.45$), traffic flow stability deteriorates and congestion progressively worsens with decreasing parameter $f$. These conclusions align with those obtained under $\gamma = 0.02$ conditions, thus leading to the following findings: The LCAIC parameter $f$ exerts significant influence on traffic flow stability in multi-lane systems. Specifically, aggressive lane-changing improves traffic stability when the overtaking rate is low but may induce negative impacts when the overtaking rate becomes high.

The Influence of LCAIC parameter $f$ on traffic flux in a multi-lane system with varying overtaking rates is illustrated in Figures 15 and 16. Specifically, Figure 15 depicts the traffic flux fluctuations at the 25th lattice point (observation point) during the initial 200 time steps and the subsequent period from 10,000 to 10,300 time steps, when the overtaking rate is low ($\lambda = 0.06$). Figure 15 reveals that, due to the violation of the traffic stability condition (20),

minor disturbances rapidly spread and intensify among vehicles, resulting in significant traffic flux fluctuations within a short timeframe (200 time steps) on the observed road segment. Even after a prolonged period of road system operation, these flux fluctuations persist and do not dissipate. Notably, as the LCAIC parameter $f$ decreases, the amplitude of these flux fluctuations gradually diminishes. This suggests that, in a multi-lane system with a low overtaking rate, more aggressive lane-changing behavior by drivers can actually help stabilize the traffic flux.

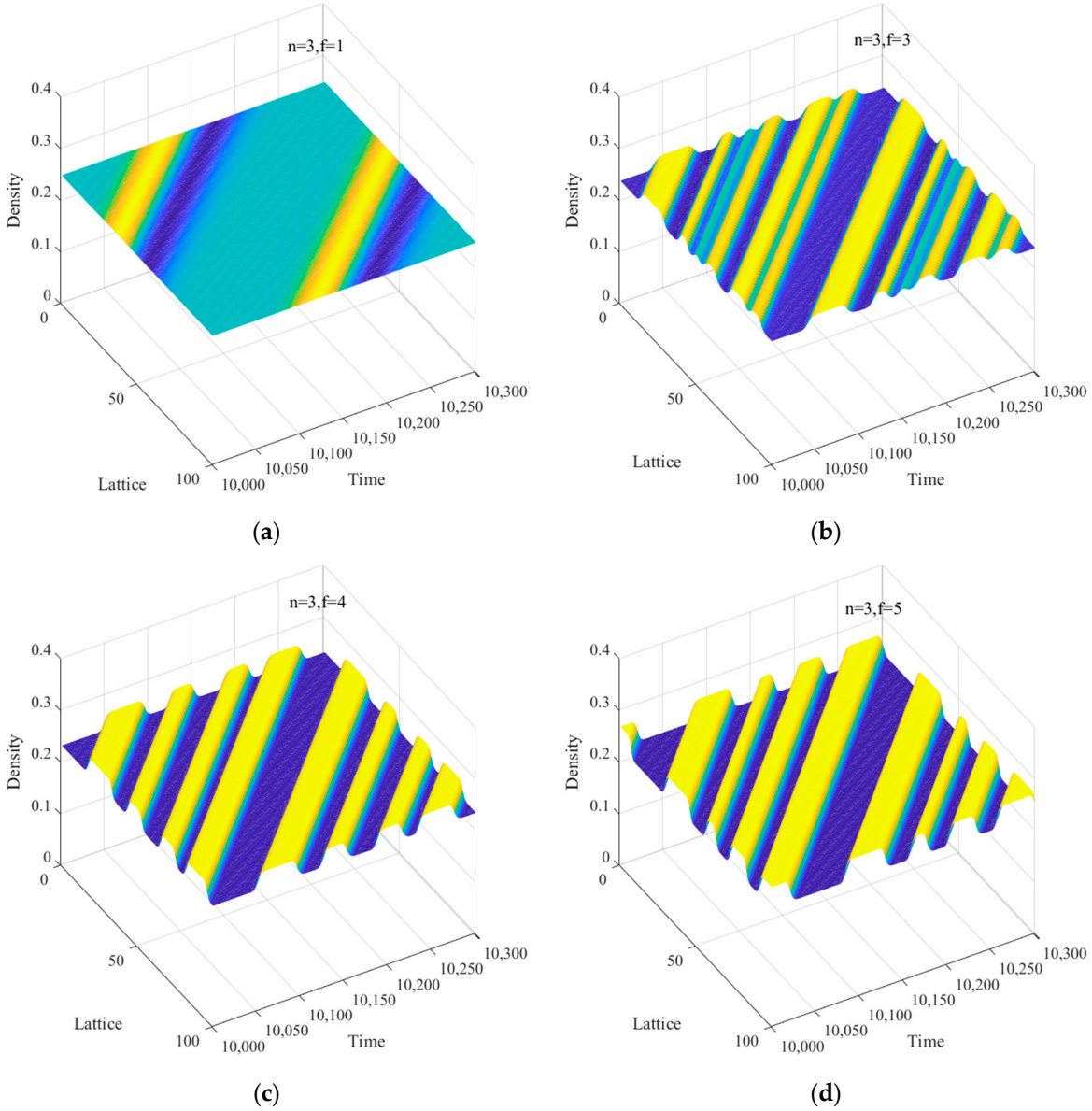



**Figure 9.** Space–time evolution of the density after t = 10,000 with $a = 3.15$, $n = 3$. The patterns (**a**), (**b**), (**c**), and (**d**) with $\lambda = 0.06$ are for $f = 1,\ 3,\ 4,\ 5$, respectively.

When the overtaking passing rate is high ($\lambda = 0.45$), we can see the traffic flow fluctuation scenarios in Figure 16 that correspond to various parameters f, where subfigures (a) and (b) depict the evolution of traffic flow during the system's first 200 time steps and the 10000-10300 time steps after full evolution, respectively. In contrast to Figure 15, the fluctuations of the traffic flow become more drastic, and the magnitude of the fluctuations significantly increases as the parameter f decreases when the overtaking passing rate is high. This reveals that under high overtaking passing rates, the more aggressive lane-changing behavior of drivers has a negative effect on the stability of multi-lane

traffic flow, i.e., it is more detrimental to the stable operation of the multi-lane traffic system. When the overtaking rate is high ($\lambda = 0.45$), Figure 16 depicts various scenarios of traffic flow fluctuations corresponding to different values of the parameter f. Specifically, subfigures (a) and (b) illustrate the evolution of traffic flow during the first 200 time steps and the period from the 10,000th to the 10,300th time step, respectively. In comparison to Figure 13, the fluctuations in traffic flow become more pronounced, and their amplitude significantly increases as the value of f decreases, especially at high overtaking rates. This highlights that drivers' more aggressive lane-changing behavior adversely affects the stability of multi-lane traffic flow, posing a greater threat to the smooth operation of the system.

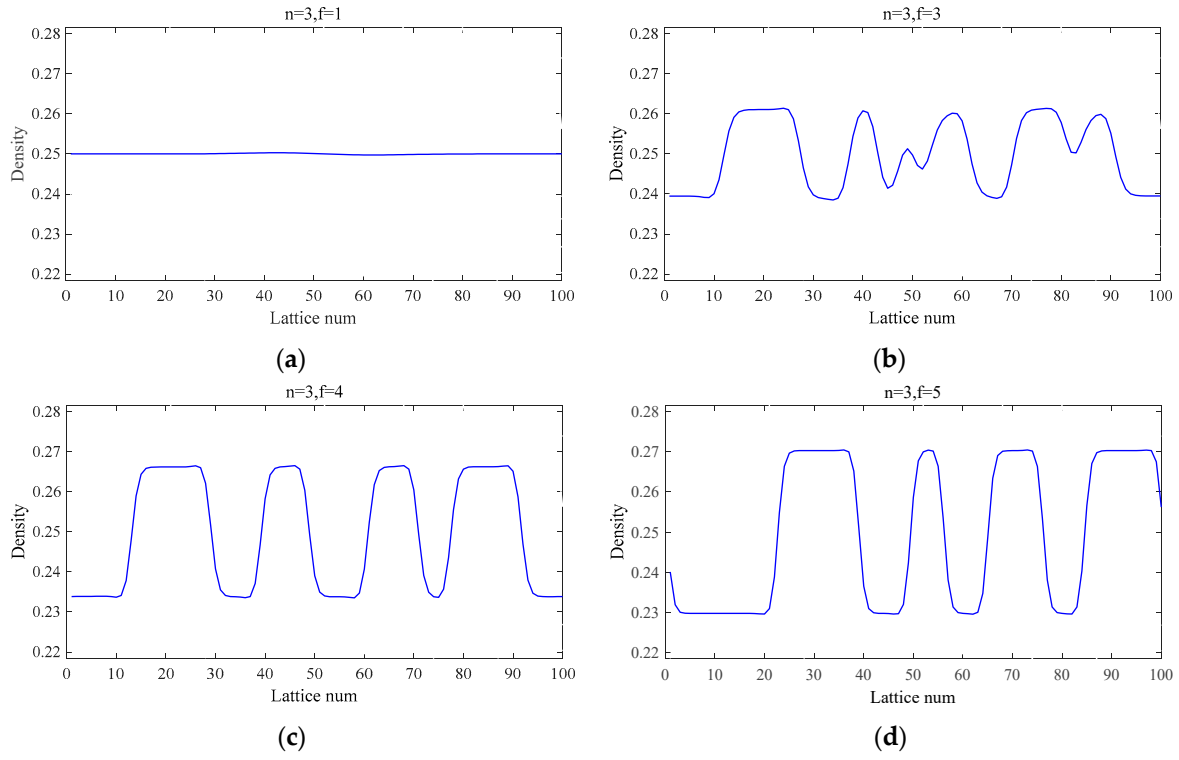



**Figure 10.** (**a**–**d**) Density profiles of the density wave at t = 10,300 correspond to the panels in Figure 9.

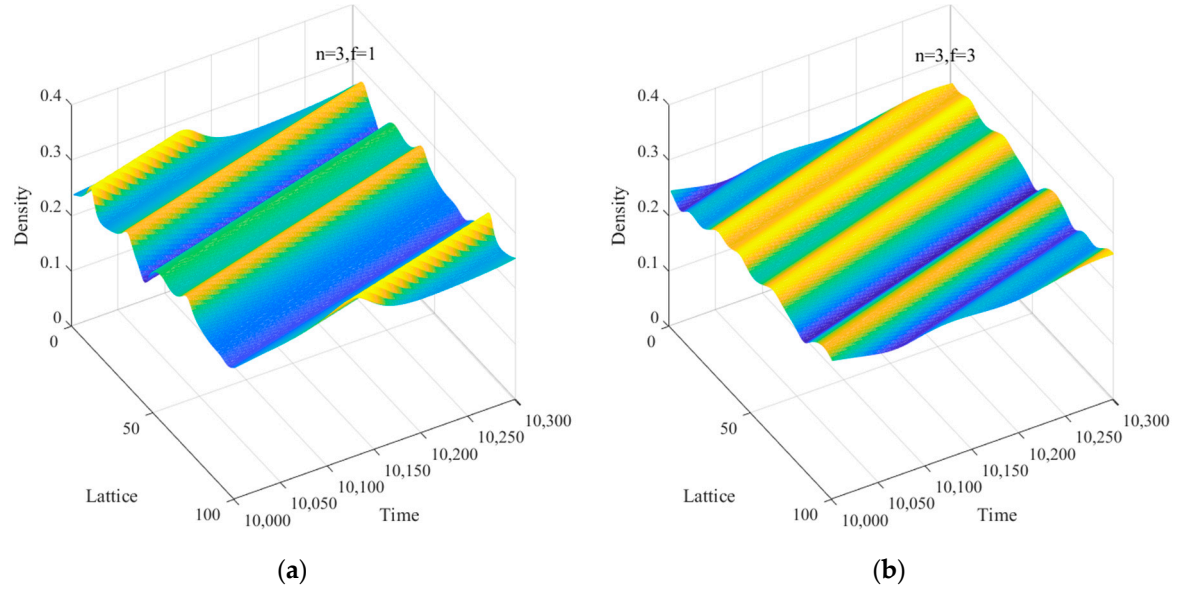
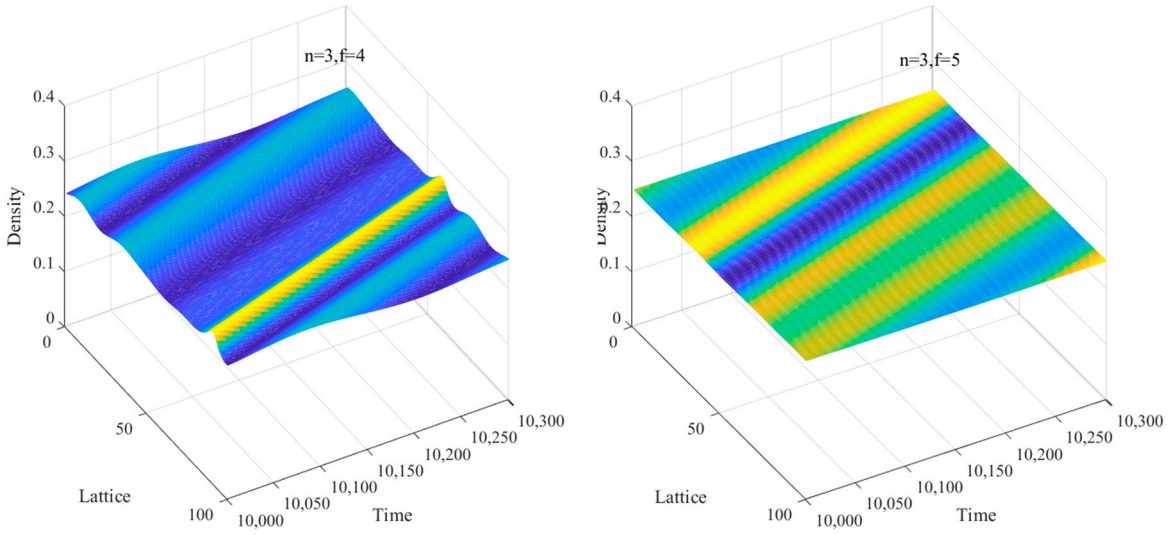


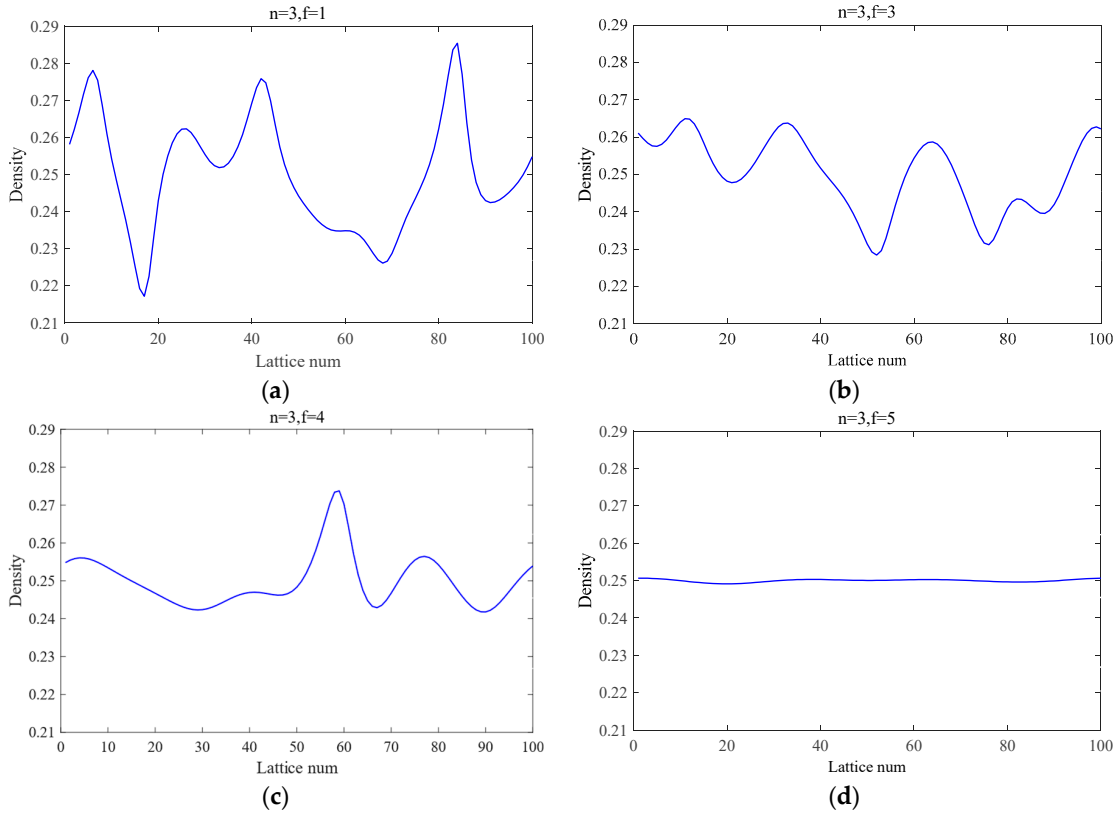

**Figure 11.** *Cont.*




(**c**) (**d**)

**Figure 11.** Space–time evolution of the density after t = 10,000 with $a = 10.5$, $n = 3$. The patterns (**a**), (**b**), (**c**), and (**d**) with $\lambda = 0.45$ are for $f = 1,\ 3,\ 4,\ 5$, respectively.

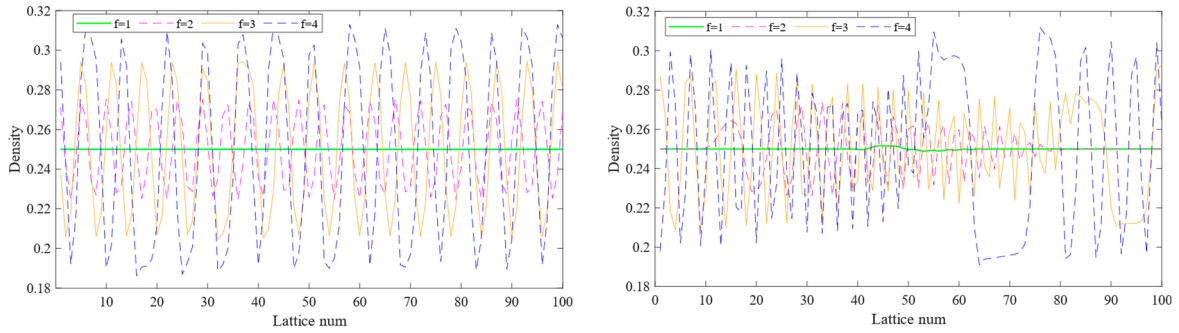
The stark contrast between Figures 15 and 16 reveals the complex dynamics resulting from the combination of aggressive lane-changing behaviors and overtaking mechanisms in the multi-lane system. Specifically, when drivers consistently adopt aggressive lane-changing strategies, the impact on the system's flow stability significantly varies depending on the overtaking rates. At low overtaking rates, these strategies actually contribute to maintaining flow stability; however, as the overtaking rate rises to a high level, they become detrimental factors that hinder flow stability.




(**a**) (**b**)

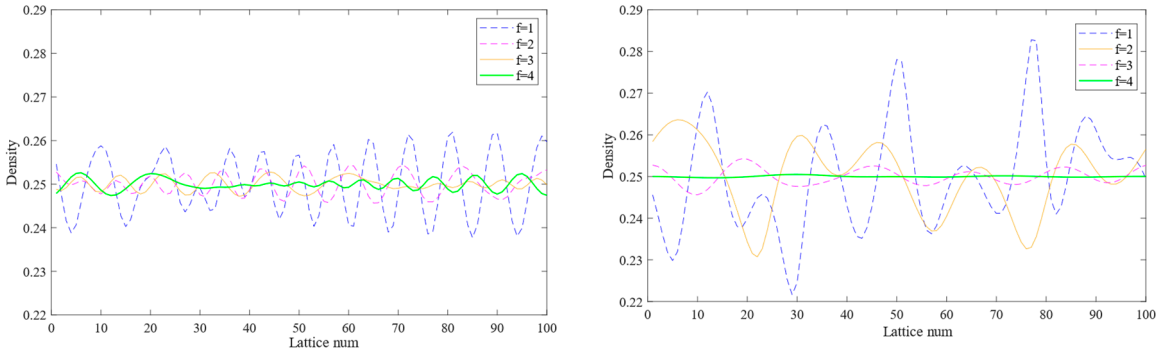
(**c**) (**d**)

**Figure 12.** (**a**–**d**) Density profiles of the density wave at t = 10,300 correspond to the panels in Figure 11.



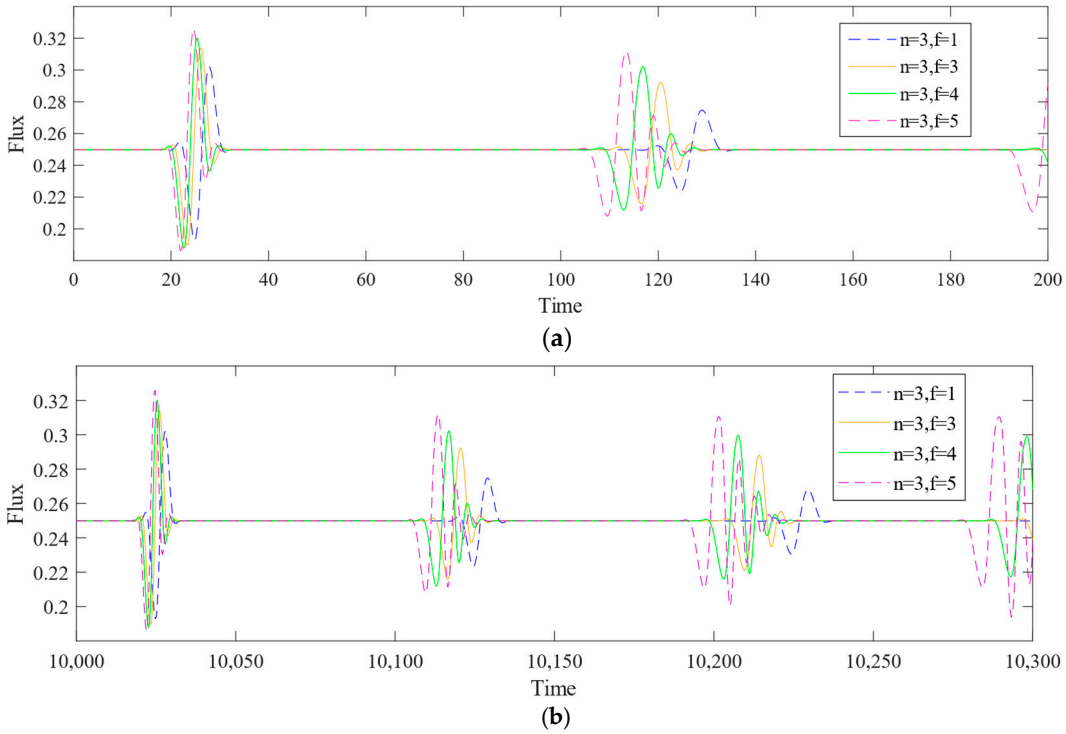

(**a**) (**b**)

**Figure 13.** Density profiles of the density wave under a different value of $f$ with $\gamma = 0.1$, $a = 2.5$, $n = 3$, and $\lambda = 0.06$. The patterns (**a**) and (**b**) correspond to t = 200 and t = 10,300, respectively.




(**a**) (**b**)

**Figure 14.** Density profiles of the density wave under a different value of $f$ with $\gamma = 0.1$, $a = 5.25$, $n = 3$, and $\lambda = 0.45$. The patterns (**a**) and (**b**) correspond to t = 200 and t = 10,300, respectively.




(**a**)

(**b**)

**Figure 15.** As $\lambda = 0.06$, the flux evolution of the 25th lattice site with $a = 3.15$, $n = 3$. The patterns (**a**) and (**b**) correspond to t = 0–200 steps and t = 10,000–10,300 steps, respectively.

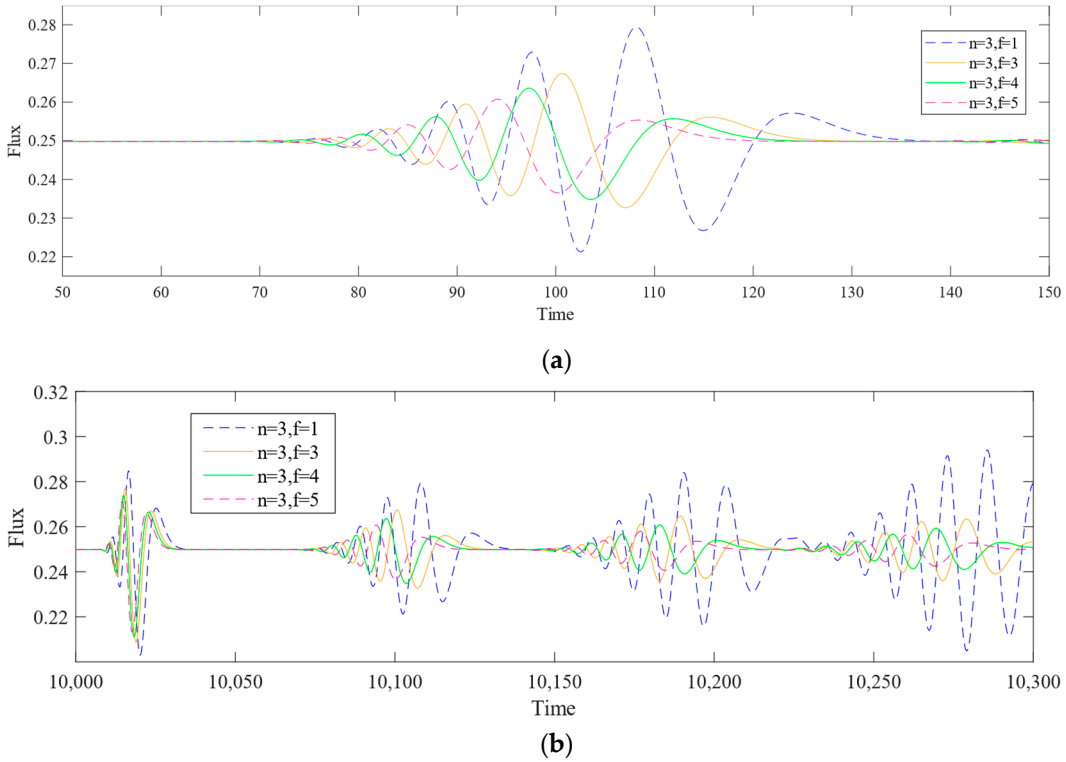



**Figure 16.** As $\lambda = 0.45$, the flux evolution of the 25th lattice site with $a = 10.5$, $n = 3$. The patterns (**a**) and (**b**) correspond to t = 0–200 steps and t = 10,000–10,300 steps, respectively.

## 6. Conclusions

The stability of traffic flow in multi-lane highway systems is greatly impacted by drivers' aggressive lane-changing and overtaking behaviors. To fully account for the combined effects of these two factors on macroscopic traffic flow, this study develops an improved multi-lane lattice traffic flow model. By refining the lane-switching protocols based on the actual level of drivers' aggression during lane changes, the new model effectively addresses the issue of oversimplification of the lane-switching mechanism in traditional lattice models, thereby bringing it closer to real-world traffic conditions. Through linear stability analysis, we established the linear stability criterion governing our proposed model. Subsequent nonlinear perturbation methods yielded the mkdv equation that characterizes the propagation and evolution of traffic jams near the critical stability point, complete with corresponding density wave solutions. Validation through extensive numerical simulations under cyclic boundary conditions demonstrated strong consistency between numerical outcomes and analytical predictions, proving the validity and accuracy of the new model. Our findings reveal contrasting efficacy profiles for aggressive lane-shifting tactics across varying overtaking frequency regimes. Specifically, when the passing rate is low, the driver's aggressive lane-changing strategy can significantly enhance the stability of the traffic flow on a multi-lane system and effectively suppress traffic flow fluctuations. However, in the context of higher overtaking passing rates, such aggressive lane-switching actions instead adversely affect the stability of the system and increase traffic flow fluctuations, i.e., the stability of the traffic flow decreases and the magnitude of traffic flow fluctuations increases as the degree of aggressive lane-changing increases. In addition, it is found that increasing the number of lanes effectively enhances the stability of traffic flow in multi-lane systems regardless of the overtaking passing rate, effectively controlling the fluctuation and propagation of traffic congestion.

However, the proposed multi-lane lattice model assumes homogeneous driver behavior. However, real-world traffic scenarios involve heterogeneous driver populations,

including aggressive and timid drivers coexisting in mixed traffic environments. Future research will extend the current model by incorporating heterogeneous driver distributions to improve its alignment with empirical observations. Furthermore, this study does not account for environmental factors such as traffic disruptions caused by accidents or weather conditions. Subsequent work will integrate these elements from a feedback control perspective to develop a comprehensive multi-lane traffic model, thereby enhancing the model's generalizability and practical utility.

**Author Contributions:** Conceptualization, S.Y. and B.H.; methodology, S.Y. and C.T.; software, Y.K.; validation, S.Y. and B.H.; formal analysis, C.T.; writing—original draft preparation, S.Y.; writing—review and editing, B.H; visualization, Y.K.; supervision, B.H.; funding acquisition, S.Y. and C.T. All authors have read and agreed to the published version of the manuscript.

**Funding:** This paper is supported by the 2023 Guizhou University of Commerce School-level Funding Project (No:2023ZKZD002) and the Special Research Project on "Studying and Interpreting the Spirit of the Third Plenary Session of the 20th CPC Central Committee" (No. 2024XJSDZD11).

**Data Availability Statement:** No data were used for the research described in this article.

**Conflicts of Interest:** The authors declare no conflict of interest.

## Appendix A

In this appendix, we present detailed derivations of the key steps leading to Equation (24). By substituting Equations (22) and (23) into the density evolution Equation (12) and performing a Taylor expansion up to the fifth order of $\varepsilon^5$, the critical components of Equation (12) are expanded as follows:

$$\rho_j(t+2\tau) = h_c + \varepsilon R + 2\varepsilon^2\tau b\partial_X R + 2\tau\varepsilon^4\partial_T R + 4\tau^2 b\varepsilon^5\partial_X\partial_T R + 2(\tau b)^2\varepsilon^3\partial_X^2 R + \tfrac{4}{3}(\tau b)^3\varepsilon^4 + \tfrac{2}{3}\partial_X^4 R(\tau b)^4\varepsilon^5 \tag{A1}$$

$$\rho_j(t+\tau) = \rho_c + \varepsilon R + \varepsilon^2\tau b\partial_X R + \tau\varepsilon^4\partial_T R + \tau^2 b\varepsilon^5\partial_X\partial_T R + \tfrac{1}{2}(\tau b)^2\varepsilon^3\partial_X^2 R + \tfrac{1}{6}(\tau b)^3\varepsilon^4 + \tfrac{1}{24}\partial_X^4 R(\tau b)^4\varepsilon^5 \tag{A2}$$

$$\rho_{j+1}(t+\tau) = \rho_c + \varepsilon R + (1+b\tau)\varepsilon^2\partial_X R + \varepsilon^4\tau\partial_T R + (1+b\tau)\varepsilon^5\tau\partial_X\partial_T R + \tfrac{1}{2}(1+b\tau)^2\varepsilon^3\partial_X^2 R + \tfrac{1}{6}(1+b\tau)^3\varepsilon^4\partial_X^3 R + \tfrac{1}{24}(1+b\tau)^4\varepsilon^5\partial_X^4 R] \tag{A3}$$

$$\rho_{j-1}(t+\tau) = \rho_c + \varepsilon R + (b\tau-1)\varepsilon^2\partial_X R + \varepsilon^4\tau\partial_T R + (b\tau-1)\varepsilon^5\tau\partial_X\partial_T R + \tfrac{1}{2}(b\tau-1)^2\varepsilon^3\partial_X^2 R + \tfrac{1}{6}(b\tau-1)^3\varepsilon^4\partial_X^3 R + \tfrac{1}{24}(b\tau-1)^4\varepsilon^5\partial_X^4 R] \tag{A4}$$

$$V(\rho_j(t)) = V(\rho_c) + V'\varepsilon R + \frac{1}{3!}V'''\varepsilon^3 R^3 \tag{A5}$$

$$V(\rho_{j+1}(t)) = V(\rho_c) + V'\varepsilon[R + \varepsilon\partial_X R + \tfrac{1}{2!}\varepsilon^2\partial_X^2 R + \tfrac{1}{3!}\varepsilon^3\partial_X^3 R + \tfrac{1}{4!}\varepsilon^4\partial_X^4 R] + \tfrac{1}{3!}V'''\varepsilon^3[R^3 + \varepsilon\partial_X R^3 + \tfrac{1}{2!}\varepsilon^2\partial_X^2 R^3] \tag{A6}$$

$$V(\rho_{j+2}(t)) = V(\rho_c) + V'\varepsilon[R + 2\varepsilon\partial_X R + 2\varepsilon^2\partial_X^2 R + \tfrac{4}{3}\varepsilon^3\partial_X^3 R + \tfrac{2}{3}\varepsilon^4\partial_X^4 R] + \tfrac{1}{6}V'''\varepsilon^3[R^3 + 2\varepsilon\partial_X R^3 + 2\varepsilon^2\partial_X^2 R^3] \tag{A7}$$

By substituting Equations (A1)–(A7) into Equation (12) and combining like terms, Equation (24) can be derived.

## References

1. Harrou, F.; Zeroual, A.; Hittawe, M.M.; Sun, Y. Road traffic modeling. In *Road Traffic Modeling and Management*; Elsevier: Amsterdam, The Netherlands, 2022; pp. 15–63.
2. Liu, K.Y.; Feng, T.J. Heterogeneous traffic flow cellular automata model mixed with intelligent controlled vehicles. *Physica A* **2023**, *632*, 129316. [CrossRef]

3. Fukui, M.; Ishibashi, Y. Traffic flow in 1d cellular automaton model including cars moving with high speed. *J. Phys. Soc. Jpn.* **1996**, *65*, 1868–1870. [CrossRef]
4. Zhai, C.; Wu, W.T.; Xiao, Y.P. Cooperative car-following control with electronic throttle and perceived headway errors on gyroidal roads. *Appl. Math. Model.* **2022**, *108*, 770–786. [CrossRef]
5. Peng, G.H.; Li, X.H.; Tan, H.L. Integrating the safety control against cyber-attacks on the global Information in coupled map car-following model under connected vehicles platoon environment. *IEEE Trans. Intell. Transp. Syst.* **2024**, *25*, 13914–13925. [CrossRef]
6. Zhai, C.; Wu, W.T. A continuous traffic flow model considering predictive headway variation and preceding vehicle's taillight effect. *Physica A* **2021**, *584*, 126364. [CrossRef]
7. Zhai, C.; Wu, W.; Xiao, Y.P. Non-lane-discipline-based continuum model considering the effect of lateral gaps and electronic throttle dynamics. *Chin. J. Phys.* **2023**, *83*, 253–269. [CrossRef]
8. Jiang, R.; Wu, Q.S.; Zhu, Z.J. A new continuum model for traffic flow and numerical tests. *Transp. Res. B* **2002**, *36*, 405–419. [CrossRef]
9. Nagatani, T. Modified KdV equation for jamming transition in the continuum models of traffic. *Physica A* **1998**, *261*, 599. [CrossRef]
10. Nagatani, T. Jamming transitions and the modified Korteweg–de Vries equation in a two-lane traffic flow. *Physica A* **1999**, *265*, 297. [CrossRef]
11. Wang, T.; Zang, R.D.; Xu, K.Y.; Zhang, J. Analysis of predictive effect on lattice hydrodynamic traffic flow model. *Physica A* **2019**, *526*, 120711. [CrossRef]
12. Kaur, D.; Sharma, S. A new two-lane lattice model by considering predictive effect in traffic flow. *Physica A* **2020**, *539*, 122913. [CrossRef]
13. Kang, Y.R.; Tian, C. A new curved road lattice model integrating the multiple prediction effect under V2X environment. *Physica A* **2024**, *643*, 129812. [CrossRef]
14. Zhai, C.; Wu, W.T.; Xiao, Y.P. An extended multi-lane lattice hydrodynamic model considering the predictive effect of drivers under connected vehicle environment. *J. Transp. Eng. Part A Syst.* **2023**, *149*, 04023099. [CrossRef]
15. Redhu, P.; Siwach, V. An extended lattice model accounting for traffic jerk. *Physica A* **2018**, *492*, 1473–1480. [CrossRef]
16. Wang, T.; Cheng, R.J.; Ge, H.X. An extended two-lane lattice hydrodynamic model for traffic flow on curved road with passing. *Physica A* **2019**, *533*, 121915. [CrossRef]
17. Jin, Y.D.; Zhou, J.; Shi, Z.K.; Zhang, H.L.; Wang, C.P. Lattice hydrodynamic model for traffic flow on curved road with passing. *Nonlinear Dyn.* **2017**, *89*, 107. [CrossRef]
18. Peng, G.H.; Kuang, H.; Zhao, H.; Li, Q. Nonlinear analysis of a new lattice hydrodynamic model with the consideration of honk effect on flux for two-lane highway. *Physica A* **2019**, *515*, 93–101. [CrossRef]
19. Peng, G.H.; Kuang, H.; Bai, K.Z. The impact of the individual difference on traffic flow under honk environment in lattice hydrodynamic model. *Physica A* **2019**, *526*, 120772. [CrossRef]
20. Wang, Q.Y.; Ge, H.X. An improved lattice hydrodynamic model accounting for the effect of "backward looking" and flow integral. *Physica A* **2019**, *513*, 438–446. [CrossRef]
21. Ge, H.X.; Cheng, R.J. The "backward looking" effect in the lattice hydrodynamic model. *Physica A* **2008**, *387*, 6952. [CrossRef]
22. Qi, X.Y.; Ge, H.X.; Cheng, R.J. Analysis of a novel lattice hydrodynamic model considering density integral and "backward looking" effect. *Physica A* **2019**, *525*, 714–723. [CrossRef]
23. Mei, Y.R.; Zhao, X.Q.; Qian, Y.Q.; Xu, S.Z.; Li, Z.P. Effect of self-stabilizing control in lattice hydrodynamic model with on-ramp and off-ramp. *Physica A* **2021**, *575*, 126048. [CrossRef]
24. Zhang, G.; Sun, D.H.; Zhao, M. Phase transition of a new lattice hydrodynamic model with consideration of on-ramp and off-ramp. *Commun. Nonlinear Sci. Numer. Simul.* **2018**, *54*, 347–355. [CrossRef]
25. Jiang, C.T.; Cheng, R.J.; Ge, H.X. Mean-field flow difference model with consideration of onramp and off-ramp. *Physica A* **2019**, *513*, 465–476. [CrossRef]
26. Tian, C.; Kang, Y.R. Modeling and optimal congestion control of multi-lane highway traffic with on-ramp and off-ramp under V2X environment. *Physica A* **2025**, *661*, 130409. [CrossRef]
27. Long, Y.; Zhang, M.; Yang, S.H.; Peng, G.H. A new lattice model integrating the flux limit effect under V2X environment. *Physica A* **2022**, *589*, 126609. [CrossRef]
28. Li, Y.X.; Zhou, T.; Peng, G.H. The dynamic evolution integrating the flux limit effect in lattice hydrodynamic model on two lanes under V2X environment. *Physica A* **2023**, *626*, 129030. [CrossRef]
29. Peng, G.H.; Zhao, H.Z.; Li, X.Q. The impact of self-stabilization on traffic stability considering the current lattice's historic flux for two-lane freeway. *Physica A* **2019**, *515*, 31–37. [CrossRef]
30. Zhang, G. The self-stabilization effect of lattice's historical flow in a new lattice hydrodynamic model. *Nonlinear Dyn.* **2018**, *91*, 809–817. [CrossRef]

31. Wang, Q.Y.; Cheng, R.J.; Ge, H.X. A novel lattice hydrodynamic model accounting for driver's memory effect and the difference of optimal velocity on curved road. *Physica A* **2020**, *559*, 125023. [CrossRef]
32. Li, L.X.; Cheng, R.J.; Ge, H.X. New feedback control for a novel two-dimensional lattice hydrodynamic model considering driver's memory effect. *Phys. A Stat. Mech. Its Appl.* **2021**, *561*, 125295. [CrossRef]
33. Zhai, C.; Wu, W.T. Stability analysis of two-lane lattice hydrodynamic model considering lane-changing and memorial effects. *Mod. Phys. Lett. B* **2018**, *32*, 1850233. [CrossRef]
34. Zhai, C.; Wu, W.T. A extended multi-phase lattice model with consideration of optimal current changes with memory. *Clust. Comput.* **2018**, *22*, 7447–7457. [CrossRef]
35. Zhang, Y.; Wang, S.; Pan, D.B.; Zhang, G. Stability analysis for a new lattice hydrodynamic model with time-varying delay in sensing traffic flux. *Phys. A Stat. Mech. Its Appl.* **2021**, *561*, 125269. [CrossRef]
36. Peng, G.H.; Jia, T.T.; Kuang, H. Energy consumptionin a new lattice hydrodynamic model based on the delayed effect of collaborative information transmission under V2X environment. *Physica A* **2022**, *585*, 126443. [CrossRef]
37. Pan, D.B.; Zhang, G.; Jiang, S.; Zhang, Y.; Cui, B.Y. Delay-independent traffic flux control for a discrete-time lattice hydrodynamic model with time-delay. *Physica A* **2021**, *563*, 125440. [CrossRef]
38. Zhao, H.Z.; Xia, D.X.; Yang, S.H.; Peng, G.H. The delayed-time effect of traffic flux on traffic stability for a two-lane freeway. *Physics A* **2020**, *540*, 123066. [CrossRef]
39. Zhai, C.; Wu, W.T. Designing continuous delay feedback control for lattice hydrodynamic model under cyber-attacks and connected vehicle environment. *Commun. Nonlinear Sci. Numer. Simul.* **2021**, *95*, 105667. [CrossRef]
40. Sharma, S. Modeling and analyses of driver's characteristics in a traffic system with passing. *Nonlinear Dyn.* **2016**, *86*, 2093. [CrossRef]
41. Peng, G.H.; Bai, K.Z.; Kuang, H. Feedback control caused by honk effect incorporating the driver's characteristics in lattice hydrodynamic model. *Physica A* **2019**, *526*, 121064. [CrossRef]
42. Zhang, G.; Sun, D.H.; Liu, W.N.; Zhao, M.; Cheng, S.L. Analysis of two-lane lattice hydrodynamic model with consideration of drivers'characteristics. *Physica A* **2015**, *422*, 16–24. [CrossRef]
43. Peng, G.H.; Kuang, H.; Qing, L. A new lattice model of traffic flow considering driver's anticipation effect of the traffic interruption probability. *Physica A* **2018**, *507*, 374. [CrossRef]
44. Redhu, P.; Gupta, A.K. Jamming transitions and the effect of interruption probability in a lattice traffic flow model with passing. *Physica A* **2015**, *421*, 249. [CrossRef]
45. Wang, Q.Y.; Cheng, R.J.; Ge, H.X. A new lattice hydrodynamic model accounting for the traffic interruption probability on a gradient highway. *Phys. Lett. A* **2019**, *383*, 1879–1887. [CrossRef]
46. Zhu, C.Q.; Zhong, S.Q.; Ma, S.F. Two-lane lattice hydrodynamic model considering the empirical lane-changing rate. *Commun. Nonlinear Sci. Numer. Simul.* **2019**, *73*, 229–243. [CrossRef]
47. Sun, F.X.; Chow, H.F.; Lo, S.M.; Ge, H.X. A two-lane lattice hydrodynamic model with heterogeneous lane changing rates. *Phys. A Stat. Mech. Its Appl.* **2018**, *511*, 389–400. [CrossRef]
48. Sun, D.H.; Liu, H.; Zhang, G. A new lattice hydrodynamic model with the consideration of flux change rate effect. *Nonlinear Dyn.* **2018**, *92*, 351–358. [CrossRef]
49. Yang, S.H.; Li, C.G.; Tang, X.L.; Tian, C. Effect of optimal estimation of flux difference information on the lattice traffic flow model. *Physica A* **2016**, *463*, 394–399. [CrossRef]
50. Peng, G.H.; Yang, S.H.; Xia, D.X.; Li, X.Q. A novel lattice hydrodynamic model considering the optimal estimation of flux difference effect on two-lane highway. *Physica A* **2018**, *506*, 929–937. [CrossRef]
51. Tian, C.; Sun, D.; Zhang, M. Nonlinear analysis of lattice model with consideration of optimal current difference. *Commun. Nonlinear Sci. Numer. Simul.* **2011**, *16*, 4524–4529. [CrossRef]
52. Peng, G.H. A new lattice model of two-lane traffic flow with the consideration of optimal current difference. *Commun. Nonlinear Sci. Numer. Simul.* **2013**, *18*, 559–566. [CrossRef]
53. Kang, Y.R.; Sun, D.H. Lattice hydrodynamic traffic flow model with explicit driver's physical delay. *Nonlinear Dyn.* **2013**, *71*, 531–537. [CrossRef]
54. Ge, H.X.; Zheng, P.J.; Lo, S.M.; Cheng, R.J. TDGL equation in lattice hydrodynamic model considering driver's physical delay. *Nonlinear Dyn.* **2014**, *76*, 441–445. [CrossRef]
55. Madaan, N.; Sharma, S. A lattice model accounting for multi-lane traffic system. *Physica A* **2021**, *564*, 125446. [CrossRef]
56. Madaan, N.; Sharma, S. Delayed-feedback control in multi-lane traffic system. *Physica A* **2022**, *599*, 127393. [CrossRef]
57. Zhai, C.; Wu, W.T.; Xiao, Y.P. The jamming transition of multi-lane lattice hydrodynamic model with passing effect. *Chaos Solitons Fractals* **2023**, *171*, 113515. [CrossRef]
58. Tian, C.; Yang, S.; Kang, Y. A novel two-lane lattice model considering the synergistic effects of drivers' smooth driving and aggressive lane-changing behaviors. *Symmetry* **2024**, *16*, 1430. [CrossRef]

59. Li, Z.P.; Zhang, R.; Xu, S.Z.; Qian, Y.Q. Study on the effects of driver's lane-changing aggressiveness on traffic stability from an extended two-lane lattice model. *Commun. Nonlinear Sci. Numer. Simul.* **2015**, *24*, 52–63. [CrossRef]
60. Ge, H.X.; Cheng, R.J.; Dai, S.Q. KdV and kink-antikink solitons in car-following models. *Physica A* **2005**, *357*, 466. [CrossRef]

**Disclaimer/Publisher's Note:** The statements, opinions and data contained in all publications are solely those of the individual author(s) and contributor(s) and not of MDPI and/or the editor(s). MDPI and/or the editor(s) disclaim responsibility for any injury to people or property resulting from any ideas, methods, instructions or products referred to in the content.